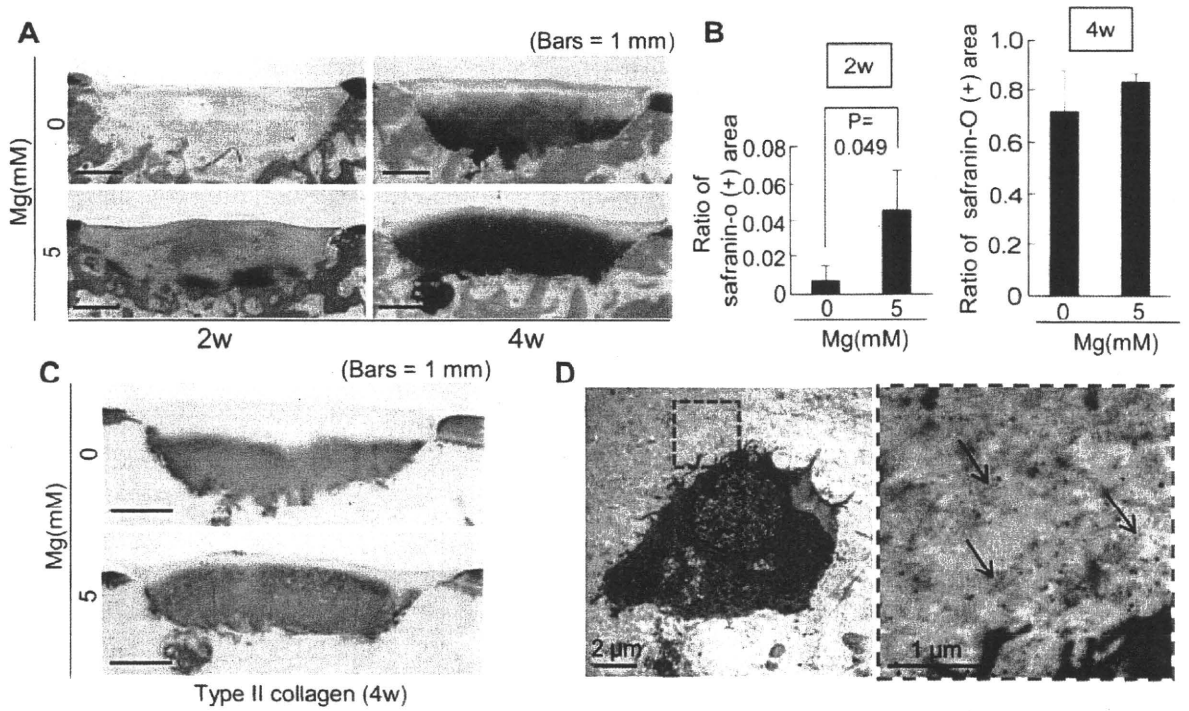

Fig. 5. *In vivo* analyses for magnesium effects on cartilage regeneration with rabbit synovial MSCs. (A) Sagittal section of defects stained with safranin-o at 2 and 4 weeks. (B) Ratio of safranin-o positive area to the total defect area at 2 and 4 weeks. Values are means with 95% CI ($n = 3$). (C) Immunohistochemistry for type II collagen at 4 weeks. (D) Transmission electron microscopic image of cell in regenerated cartilage of rabbit treated with synovial MSCs suspended in PBS at 4 weeks (left) and the magnified image (right). The arrows indicate collagen fibrils.

analysis. Intra-articular circumstance caused a discomfort condition for MSCs to continue in their attachment to osteochondral defects due to gravity force, bleeding, inflammatory reactions, and mechanical stresses accompanied with joint motions.

During *in vivo* situation, magnesium increased adherence of MSCs to the basement of the defect. Histologically, a greater number of cells accumulated on the layer of cells which were attached to the basement of the defects in the presence of magnesium. There are two possibilities to account for the result. Magnesium also may enhance accumulation of MSCs on the layer of the cells. Otherwise, a greater number of single-layered cells on the basement of defect may enhance accumulation of MSCs dependent on or independent of magnesium.

In vivo studies showed that cartilage matrix was regenerated earlier in the defects treated in the presence of 5 mM magnesium at 2 weeks. The number of cells involved in regeneration of cartilage is an important factor[33]. The difference of initial cell number attached to the defect or initial magnesium concentration may have been an

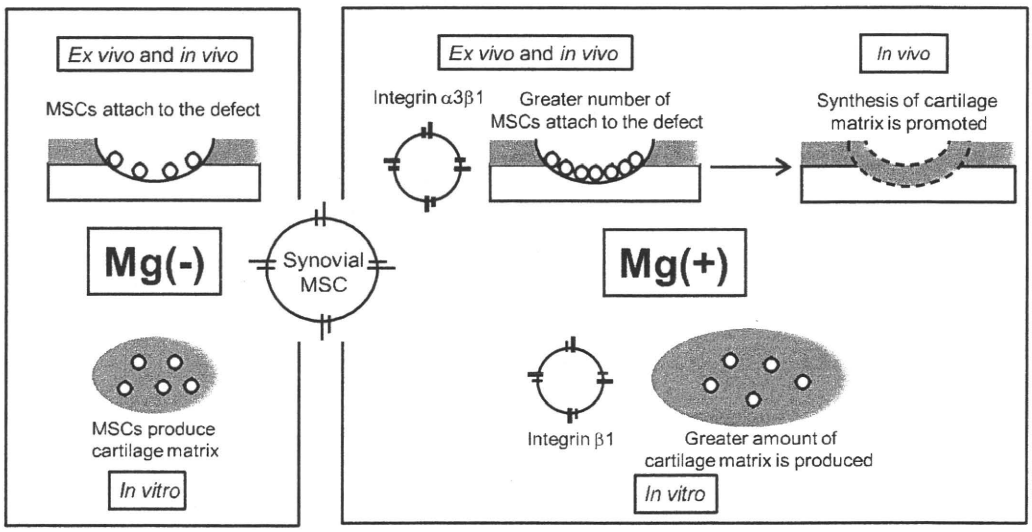

Fig. 6. Scheme of MSC based cartilage regeneration with magnesium. Magnesium increases MSC attachment and cartilage matrix formation through integrins at initial stage without toxicity.

influencing factor even after 2 weeks. As a whole, the presence of magnesium in cell suspension promoted cell adhesion to osteochondral defects and exerted no toxic effect on *in vivo* cartilage formation.

Standard media for cell culture, which also promote cell attachment, are not usually approved for clinical use. The most popular standard solution for clinical use is a lactate Ringer's solution, which does not contain magnesium. To demonstrate the effect of magnesium experimentally, we selected PBS (−), which is a more simplified standard solution close to a lactate Ringer's solution. PBS (+) contains 0.8 mM magnesium, and we showed that 5 mM magnesium had stronger effects for attachment and cartilage formation of synovial MSCs than PBS (+) containing 0.8 mM magnesium. Even if we had used PBS (+) as a control, the results would not have been significantly affected.

In summary, magnesium enhanced attachment of synovial MSCs to osteochondral defect through integrin $\alpha 3\beta 1$. A greater number of MSCs were attached to the defect and promoted synthesis of cartilage matrix at an early phase. Furthermore, magnesium increased cartilage matrix synthesis through integrin $\beta 1$ during *in vitro* chondrogenesis of synovial MSCs (Fig. 6).

Contributions

Masayuki Shimaya: conception and design, analysis and interpretation of the data, collection and assembly of data, drafting of the article; Takeshi Muneta: obtaining of funding, provision of study materials and patients; Kunikazu Tsuji: critical revision of the article for important intellectual content; Shizuko Ichinose: electron microscopy; Ichiro Sekiya: conception and design, critical revision of the article for important intellectual content, final approval of the article, obtaining of funding.

Conflict of interest

The authors have no conflict of interest.

Acknowledgement

This study was supported by grants from the Japanese Ministry of Education Global Center of Excellence (GCOE) Program, the International Research Center for Molecular Science in Tooth and Bone Diseases and from the Japan Society for the Promotion of Science (21591914) to TM and by the Japan Society for the Promotion of Science (21591914) to IS Recombinant human bone morphogenetic protein-7 was kindly provided by Stryker Biotech.

References

1. Pittenger M, Mackay A, Beck S, Jaiswal R, Douglas R, Mosca J, *et al.* Multilineage potential of adult human mesenchymal stem cells. Science 1999;284(5411):143–7.
2. Prockop D. Marrow stromal cells as stem cells for nonhematopoietic tissues. Science 1997;276(5309):71–4.
3. Sekiya I, Larson B, Smith J, Pochampally R, Cui J, Prockop D. Expansion of human adult stem cells from bone marrow stroma: conditions that maximize the yields of early progenitors and evaluate their quality. Stem Cells 2002;20(6):530–41.
4. Sakaguchi Y, Sekiya I, Yagishita K, Muneta T. Comparison of human stem cells derived from various mesenchymal tissues: superiority of synovium as a cell source. Arthritis Rheum 2005;52(8):2521–9.
5. Shirasawa S, Sekiya I, Sakaguchi Y, Yagishita K, Ichinose S, Muneta T. *In vitro* chondrogenesis of human synovium-derived mesenchymal stem cells: optimal condition and comparison with bone marrow-derived cells. J Cell Biochem 2006;97(1):84–97.
6. Yoshimura H, Muneta T, Nimura A, Yokoyama A, Koga H, Sekiya I. Comparison of rat mesenchymal stem cells derived from bone marrow, synovium, periosteum, adipose tissue, and muscle. Cell Tissue Res 2007;327(3):449–62.
7. Nimura A, Muneta T, Koga H, Mochizuki T, Suzuki K, Makino H, *et al.* Increased proliferation of human synovial mesenchymal stem cells with autologous human serum: comparisons with bone marrow mesenchymal stem cells and with fetal bovine serum. Arthritis Rheum 2008;58(2):501–10.
8. Mochizuki T, Muneta T, Sakaguchi Y, Nimura A, Yokoyama A, Koga H, *et al.* Higher chondrogenic potential of fibrous synovium- and adipose synovium-derived cells compared with subcutaneous fat-derived cells: distinguishing properties of mesenchymal stem cells in humans. Arthritis Rheum 2006;54(3):843–53.
9. Nagase T, Muneta T, Ju YJ, Hara K, Morito T, Koga H, *et al.* Analysis of the chondrogenic potential of human synovial stem cells according to harvest site and culture parameters in knees with medial compartment osteoarthritis. Arthritis Rheum 2008;58(5):1389–98.
10. Segawa Y, Muneta T, Makino H, Nimura A, Mochizuki T, Ju YJ, *et al.* Mesenchymal stem cells derived from synovium, meniscus, anterior cruciate ligament, and articular chondrocytes share similar gene expression profile. J Orthop Res 2009;27(4):435–41.
11. Brittberg M, Lindahl A, Nilsson A, Ohlsson C, Isaksson O, Peterson L. Treatment of deep cartilage defects in the knee with autologous chondrocyte transplantation. N Engl J Med 1994;331(14):889–95.
12. Wakitani S, Goto T, Pineda S, Young R, Mansour J, Caplan A, *et al.* Mesenchymal cell-based repair of large, full-thickness defects of articular cartilage. J Bone Joint Surg Am 1994;76(4):579–92.
13. Koga H, Shimaya M, Muneta T, Nimura A, Morito T, Hayashi M, *et al.* Local adherent technique for transplanting mesenchymal stem cells as a potential treatment of cartilage defect. Arthritis Res Ther 2008;10(4):R84.
14. Docheva D, Popov C, Mutschler W, Schieker M. Human mesenchymal stem cells in contact with their environment: surface characteristics and the integrin system. J Cell Mol Med 2007;11(1):21–38.
15. Hynes R. Integrins: bidirectional, allosteric signaling machines. Cell 2002;110(6):673–87.
16. Martino M, Mochizuki M, Rothenfluh D, Rempel S, Hubbell J, Barker T. Controlling integrin specificity and stem cell differentiation in 2D and 3D environments through regulation of fibronectin domain stability. Biomaterials 2009;30(6):1089–97.
17. Leitinger B, McDowall A, Stanley P, Hogg N. The regulation of integrin function by Ca2+. Biochim Biophys Acta 2000;1498(2–3):91–8.
18. Banères JL, Roquet F, Martin A, Parello J. A minimized human integrin alpha 5 beta 1 that retains ligand recognition. J Biol Chem 2000;275(8):5888–903.
19. Kirchhofer D, Grzesiak J, Pierschbacher MD. Calcium as a potential physiological regulator of integrin-mediated cell adhesion. J Biol Chem 1991;266(7):4471–7.
20. Grzesiak J, Davis G, Kirchhofer D, Pierschbacher M. Regulation of alpha 2 beta 1-mediated fibroblast migration on type I collagen by shifts in the concentrations of extracellular Mg2+ and Ca2+. J Cell Biol 1992;117(5):1109–17.
21. Ichinose S, Tagami M, Muneta T, Sekiya I. Morphological examination during *in vitro* cartilage formation by human mesenchymal stem cells. Cell Tissue Res 2005;322(2):217–26.

22. Moran DT, Rowley JC. Visual Histology. Philadelphia: Lea and Febiger; 1988.
23. Cross PC, Mercer KL. Cell and Tissue Ultrastructure: a Functional Perspective. New York: W.H. Freeman and Company; 1993.
24. Friedenstein AJ. Precursor cells of mechanocytes. Int Rev Cytol 1976;47:327–59.
25. Sekiya I, Colter DC, Prockop DJ. BMP-6 enhances chondrogenesis in a subpopulation of human marrow stromal cells. Biochem Biophys Res Commun 2001;284(2):411–8.
26. Sakaguchi Y, Sekiya I, Yagishita K, Ichinose S, Shinomiya K, Muneta T. Suspended cells from trabecular bone by collagenase digestion become virtually identical to mesenchymal stem cells obtained from marrow aspirates. Blood 2004;104(9):2728–35.
27. Song SW, Chang W, Song BW, Song H, Lim S, Kim HJ, *et al.* Integrin-linked kinase is required in hypoxic mesenchymal stem cells for strengthening cell adhesion to ischemic myocardium. Stem Cells 2009;27(6):1358–65.
28. Wayner E, Carter W. Identification of multiple cell adhesion receptors for collagen and fibronectin in human fibrosarcoma cells possessing unique alpha and common beta subunits. J Cell Biol 1987;105(4):1873–84.
29. Berdichevsky F, Alford D, D'Souza B, Taylor-Papadimitriou J. Branching morphogenesis of human mammary epithelial cells in collagen gels. J Cell Sci 1994;107(12):3557–68.
30. Carter W, Wayner E, Bouchard T, Kaur P. The role of integrins alpha 2 beta 1 and alpha 3 beta 1 in cell–cell and cell–substrate adhesion of human epidermal cells. J Cell Biol 1990;110 (4):1387–404.
31. Sekiya I, Vuoristo JT, Larson BL, Prockop DJ. *In vitro* cartilage formation by human adult stem cells from bone marrow stroma defines the sequence of cellular and molecular events during chondrogenesis. Proc Natl Acad Sci U S A 2002;99 (7):4397–402.
32. Sekiya I, Larson BL, Vuoristo JT, Reger RL, Prockop DJ. Comparison of effect of BMP-2, -4, and -6 on *in vitro* cartilage formation of human adult stem cells from bone marrow stroma. Cell Tissue Res 2005;320(2):269–76.
33. Koga H, Muneta T, Nagase T, Nimura A, Ju Y, Mochizuki T, *et al.* Comparison of mesenchymal tissues-derived stem cells for *in vivo* chondrogenesis: suitable conditions for cell therapy of cartilage defects in rabbit. Cell Tissue Res 2008;333 (2):207–15.

Threshold in Stage-specific Embryonic Glycotypes Uncovered by a Full Portrait of Dynamic *N*-Glycan Expression during Cell Differentiation*

Maho Amano‡, Misa Yamaguchi‡, Yasuhiro Takegawa‡, Tadashi Yamashita‡, Michiyo Terashima§, Jun-ichi Furukawa‡, Yoshiaki Miura¶, Yasuro Shinohara‡, Norimasa Iwasaki§, Akio Minami§, and Shin-Ichiro Nishimura‡¶‖

Although various glycoforms appear to participate independently in multiple molecular interactions in cellular adhesion that contribute to embryogenesis and organogenesis, a full portrait of the glycome diversity and the effect of the structural variations of cellular glycoforms on individual cell stages in proliferation and differentiation remain unclear. Here we describe a novel concept for the characterization of dynamic glycoform alteration during cell differentiation by means of "glycoblotting-based cellular glycomics," the only method allowing for rapid and quantitative glycan analysis. We demonstrated that processes of dynamic cellular differentiation of mouse embryonic carcinoma cells, P19CL6 and P19C6, and mouse embryonic stem cells into cardiomyocytes or neural cells can be monitored and characterized quantitatively by profiling entire *N*-glycan structures of total cell glycoproteins. Whole *N*-glycans enriched and identified by the glycoblotting method (67 glycans for P19CL6, 75 glycans for P19C6, and 72 glycans for embryonic stem cells) were profiled and bar-coded quantitatively with respect to the ratio of subgroups composed of characteristic glycoforms, namely glycotypes. ***Molecular & Cellular Proteomics 9:523–537, 2010.***

The global characterization of the genome, transcriptome, epigenome, and proteome of embryonic stem cells (ESCs)[1] has contributed to basic understanding of ESC biology (1). Functional genomics and proteomics during cellular differentiation have also been intensively studied during recent years (2–4). However, it was suggested that there is no significant change of the protein expression profile in the differentiated cells in comparison with that of undifferentiated (progenitor) cells. It is generally recognized that work on ESCs has proceeded with a general lack of standards for adequate quantification of ESCs (5). It is likely that this has led to inconsistencies and difficulties in reproducing work from independent laboratories because this field has relied upon a variety of antibodies against a few cell surface antigens, which has been useful but not adequate. Therefore, it should be noted that there has been no reliable set of molecular markers that can easily establish the quality and differentiation status of a cell line.

Numerous important roles of mammalian glycans are now evident, and the variation in the cellular glycome is a molecular basis for modulating dynamic cellular mechanisms such as cell-cell adhesion, cell activation, and malignant alterations (6–9). Structural variations of the glycome in cell surface glycoproteins and/or glycosphingolipids appear to produce some useful biomarkers such as stage-specific embryonic antigens and ligands for endogenous lectins during cell proliferation and differentiation (10–13). Loss of some key *N*-glycans or expression of unusual *N*-glycans disrupts normal cell-cell adhesion in early mammalian embryos that is associated with fertilization (14–17). In addition, it seems likely that cellular responsiveness to growth or arrest is greatly dependent on total *N*-glycan number and the degree of branching of cell surface glycoproteins (12). Judging from the fact that *N*-glycans found in most proteins are an overwhelming majority of the glycome compared with other subgroups such as *O*-glycans classified as mucin glycoproteins or glycosphingolipids, our attention should be focused on the expression profiles of cellular *N*-glycans.

We hypothesized that drastic changes in the ratio of some key subtypes of the *N*-glycans with mutual core structure against total *N*-glycan expression level may be crucial to

From the ‡Laboratory of Advanced Chemical Biology, Graduate School of Life Science, and Frontier Research Center for Post-Genome Science and Technology, Hokkaido University, N21 W11, Kita-ku, Sapporo 001-0021, Japan, §Department of Orthopedic Surgery, Hokkaido University School of Medicine, N15 W7, Kita-ku, Sapporo 060-8638, Japan, and ¶Ezose Sciences, Inc., Pine Brook, New Jersey 07058

Received, November 18, 2009, and in revised form, December 14, 2009

Published, MCP Papers in Press, December 14, 2009, DOI 10.1074/mcp.M900559-MCP200

[1] The abbreviations used are: ESC, embryonic stem cell; iPS, induced pluripotent stem; FBS, fetal bovine serum; RA, retinoic acid; HRP, horseradish peroxidase; NeuGc, *N*-glycolylneuraminic acid; HM, high mannose type; MF, monofucosylated type; DF, difucosylated type; O, others; BS, bisect type.

switch cell stages/types during cell differentiation in which generated *N*-glycan subtypes must exchange their major partner molecules in differentiated cell adhesion, namely cell surface carbohydrate-binding proteins or complementary glycans in sugar-sugar interaction (18). In other words, there might be a significant "threshold" or "critical point" in the expression level of the key *N*-glycan subtypes against cell surface area to initiate this dynamic cellular differentiation. For example, it is well documented that Lewis X trisaccharide antigen (SSEA-1), a prominent member of the Lewis blood group antigen family, is one of the most important subtypes that have key functional roles during developmental processes or cancer progression (10, 19). Glycosphingolipids SSEA-3 and SSEA-4 are also among the most commonly utilized markers to characterize ESCs, and they could also be classified as a sort of subtype composed of globoseries core oligosaccharide structures (13). Sialic acid-containing oligosaccharides are also supposed to be involved in some essential subtypes having various functions as potential markers in cell differentiation or malignant alteration (20). Therefore, it is not surprising that real time monitoring of entire *N*-glycan expression levels in the course of proliferation and differentiation, a full portrait of the cellular glycoforms, may allow for the identification of target cells and assessment of the quality of individual stem cells and differentiated cells. The advent of such a versatile and comprehensive protocol for quantitative cellular glycomics is now urgently needed because it should greatly contribute to the quality control of human ESCs and a variety of human induced pluripotent stem (iPS) cells in terms of the warranty of safety and reproducibility of required stem cell engineering (21–23).

Until now, technical limitations have restricted acquisition of the total glycan structures of mammalian cells and evaluation of the cell type-specific glycoforms (24). We report herein that the glycoblotting method (24), a PCR-like technology developed for rapid and large scale enrichment analysis of human serum glycans (25, 26), can be used for rapid and quantitative cellular glycomics to monitor dynamic glycoform alteration during differentiation of mouse embryonic carcinoma cells (P19CL6 and P19C6 cells) and mouse ESCs.

MATERIALS AND METHODS

Cell Culture and Differentiation—P19C6 and P19CL6 cells were subcloned from pluripotent mouse embryonal carcinoma, and both were obtained from RIKEN Cell Bank (Ibaragi, Japan) (27, 28). P19C6 and P19CL6 were maintained with Dulbecco's modified Eagle's medium (Sigma-Aldrich) supplemented with 15% fetal bovine serum (FBS; Biological Industries, Kibbutz Beit Haemek, Israel) and minimum Eagle's medium α supplemented with 10% FBS and penicillin-streptomycin (Invitrogen), respectively, at 37 °C in an atmosphere of 5% CO_2. P19C6 cells were differentiated as described by Tang and co-workers (29). In brief, P19 cells were cultured by the hanging drop method and allowed to aggregate in bacterial grade Petri dishes at a cell density of 1×10^5 cells/ml in the presence of 1 μM retinoic acid (RA) (Sigma) in minimum Eagle's medium α supplemented with 10% FBS. After 4 days of aggregation, cells were collected in "aggregate," an intermediate of differentiation, by treatment with 0.05% trypsin, EDTA (Invitrogen) and were replated onto a poly-L-lysine-coated tissue culture dish (6 cm inner diameter) at a density of 5×10^4 cells/cm^2 in Dulbecco's modified Eagle's medium/F-12 medium (Invitrogen) containing N-2 supplement and fibronectin. The cells were then allowed to adhere and were cultured for 5 days. Cardiac muscle differentiation of P19CL6 cells was induced by DMSO under adherent conditions as described previously (27). Briefly, 3.7×10^5 cells were plated onto a tissue culture dish (6 cm inner diameter) (Corning) and cultured in a standard medium containing 1% DMSO for 16 days. As a control, undifferentiated cells were cultured in standard medium for 16 days. The media were changed every 2 days. All experiments were performed in triplicate and repeated twice independently (n = 6). Mouse ESCs were differentiated under conditions reported previously (30, 31).

Basic Protocol of Glycoblotting-based Quantitative Cellular N-Glycomics—A preliminary trial for the cellular *N*-glycomics was reported previously in human prostate cancer cells (PC-3) and normal human prostate epithelial cells on the basis of the protocol designed for human serum *N*-glycomics using the BlotGlyco™ ABC bead, a prototype bead prepared by conjugating *N*-(2-aminobenzoyl)cysteine hydrazide and thiopropyl-Sepharose 6B (26). However, we had to re-examine and establish a comprehensive protocol feasible for mammalian cellular glycomics using BlotGlyco H, a commercially available synthetic polymer bead (Sumitomo Bakelite Co., Ltd., Tokyo, Japan) (see Fig. 1), because our recent studies on the functional glycomics using BlotGlyco H bead have demonstrated improved performance of this new platform in terms of quantification, reproducibility, and application (25).

Release of total *N*-glycans was carried out directly using whole cell lysates as follows. After inducing differentiation, P19C6 and ESCs were cultured by using a poly-L-lysine-coated tissue culture dish (6 cm inner diameter) for the appropriate days indicated above, then were scraped in PBS containing 10 mM EDTA, and washed with PBS. Following suspension in PBS, cells were lysed by incubation with 1% Triton X-100 for 1 h on ice. The lysates were centrifuged at 15,000 rpm for 10 min at 4 °C, and the obtained supernatant was added to cold acetone (1:4) to precipitate proteinaceous materials. The precipitates were collected by centrifugation at 12,000 rpm for 15 min at 4 °C followed by serial washing with acetonitrile. The resulting precipitates were dissolved in 50 μl of 80 mM ammonium bicarbonate containing 0.2% of 1-propanesulfonic acid, 2-hydroxyl-3-myristamido and incubated at 60 °C for 10 min. The solubilized proteinaceous materials were reduced by 10 mM DTT at 60 °C for 30 min followed by alkylation with 20 mM iodoacetamide by incubation in the dark at room temperature for 30 min. The mixture was then treated with 400 units of trypsin (Sigma-Aldrich) at 37 °C overnight followed by heat inactivation of the enzyme at 90 °C for 10 min. After cooling to room temperature, *N*-glycans of glycopeptides were released from trypsin-digested samples by incubation with 2 units of peptide-*N*-glycosidase F (Roche Applied Science) at 37 °C overnight. Then the sample mixture was dried by SpeedVac and stored at −20 °C until use. Approximately $1–5 \times 10^6$ cells (~200 μg of total protein) corresponding to cell confluence on the culture dish (6 cm inner diameter) were required for this procedure.

Glycoblotting of the sample mixtures containing whole cell *N*-glycans by means of BlotGlyco H bead was performed according to the procedure described previously (26). BlotGlyco H beads (500 μl) (10 mg/ml suspension; Sumitomo Bakelite Co., Ltd.) were aliquoted onto a well of a MultiScreen Solvinert filter plate (Millipore, Billerica, MA). Peptide-*N*-glycosidase F-digested samples were dissolved with 20 μl of water and applied to the well followed by the addition of 180 μl of 2% acetic acid in ACN. The plate was incubated at 80 °C for 45 min to capture total glycans in sample mixtures specifically onto

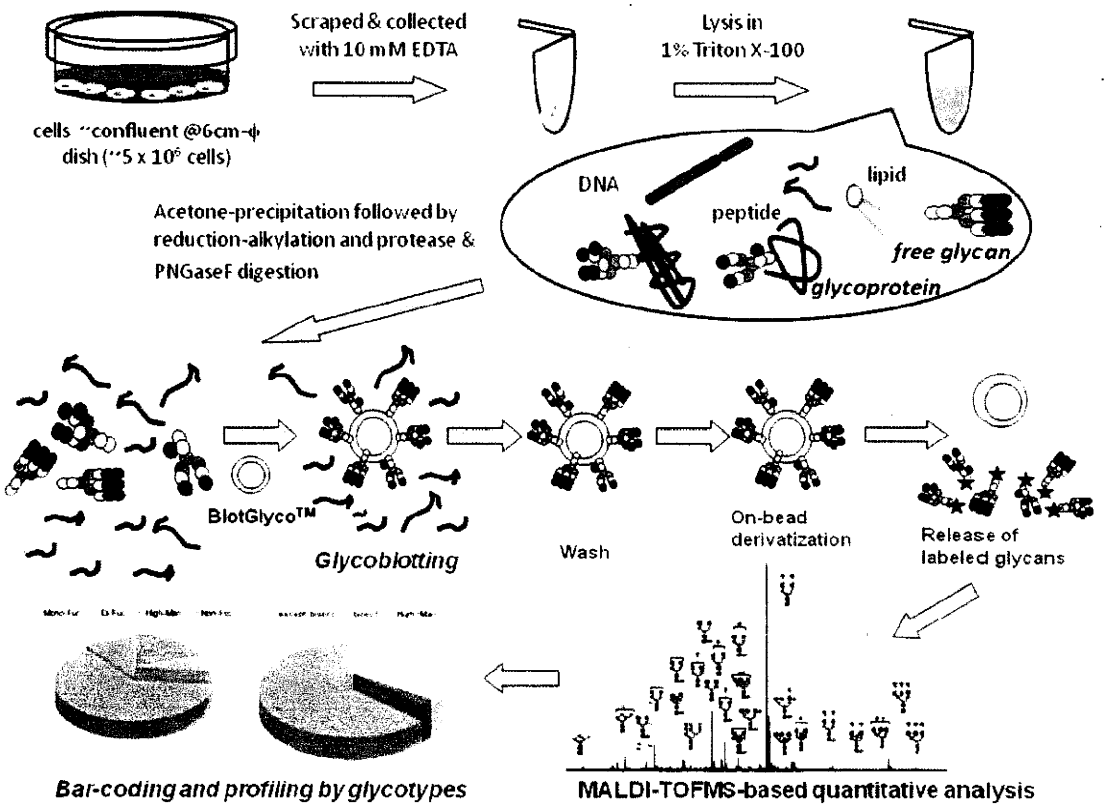

FIG. 1. **Basic protocol of high throughput and quantitative cellular glycomics based on glycoblotting method using BlotGlyco H bead.** ϕ, inner diameter; *PNGaseF*, peptide-*N*-glycosidase F.

beads via stable hydrazone bonds. The plate was washed by 200 μl of 2 M guanidine HCl in ammonium bicarbonate followed by washing with the same volume of water and 1% triethylamine in methanol (MeOH). Each washing step was performed twice, respectively. Unreacted hydrazide functional groups on beads were capped by incubation with 10% acetic anhydride in MeOH for 30 min at room temperature. Then the solution was removed by vacuum, and then the bead was serially washed by 2 × 200 μl of 10 mM HCl, MeOH, and dioxane, respectively. On-bead methyl esterification of carboxyl groups in sialic acids was carried out by incubation with 150 mM 3-methyl-1-*p*-tolyltriazene in dioxane at 60 °C to dryness. It usually took 90 min in a conventional oven. Then the bead was serially washed by 200 μl of dioxane, water, MeOH, and water. The glycans blotted on beads were subjected to the *trans*-iminization reaction with aoWR (aminooxy-functionalized peptide reagent) for 45 min at 80 °C. WR-tagged glycans were eluted by adding 100 μl of water and then purified by a Mass PREP™ hydrophilic interaction chromatography (HILIC) μElution Plate (Waters) according to the manufacturer's description.

The purified *N*-glycans were 10-fold concentrated by SpeedVac followed by direct dissolution with 2,5-dihydroxylbenzoic acid (10 mg/ml in 30% ACN) and were crystallized. Then the analytes were subjected to MALDI-TOF-MS analysis using an Ultraflex time-of-flight mass spectrometer III (Bruker Daltonics, Billerica, MA) in reflector, positive ion mode typically summing 1000 shots. The detected *N*-glycan peaks in MALDI-TOF-MS spectra were picked using the software FlexAnalysis version 3 (Bruker Daltonics) in independently performed experiments in P19C6, P19CL6, and ESCs, respectively. The intensity of the isotopic peaks of each glycan was normalized to 15 pmol of internal standard (A2 amide glycan) in each status. The changes of glycan expression levels were calculated as differentiated *versus* undifferentiated. Student's *t* test was used to calculate the statistical difference of cell status, namely differentiated *versus* undifferentiated. The glycan structures were speculated using GlycoMod Tool and GlycoSuite.

RT-PCR—RNA was extracted from 1.5–5 × 10^7 P19CL6 cells using an "R&D Quick" kit (Dainippon Sumitomo Pharma Co., Ltd., Osaka, Japan) according to the manufacturer's instructions. RT-PCR was performed using the SuperScriptIII One-Step RT-PCR System with Platinum *Taq* DNA polymerase (Invitrogen) to reverse transcribe and amplify cDNAs coding the proteins described below. The primer sequences were as follows: β-actin, 3′-TGTGATGGTGGGAATGGGTCGG-5′ and 5′-TTTGATGTCACGCACGATTTCC-3′; α-cardiac myosin heavy chain, 3′-CTGCTGGAGAGGTTATTCCTCG-5′ and 5′-GGAAGAGTGAGCGGCGCATCAAGG-3′; and β-cardiac myosin heavy chain, 3′-TGCAAAGGCTCCAGGTCTGAGGGC-5′ and 5′-GCCAACACCAACCTGTCCAAGTTC-3′).

Immunohistochemistry—Sixteen days after incubation with or without 1% DMSO, P19CL6 cells were collected as described above and dissociated intensively by EDTA/PBS containing 0.05% trypsin. After washing, cells were dissolved in PBS and smeared onto silane-coated slide glass (SUPERFROST®, Matsunami Glass, Osaka, Japan). Cells were fixed in cold acetone and treated with MeOH containing 3% H_2O_2 for 10 min at room temperature to quench internal peroxidase activity. Nonspecific binding on cells was blocked by incubation with CAS-Block (Zymed Laboratories Inc.) for 10 min at room temperature. Cells were then incubated with MF20 (1:800) (The monoclonal antibody developed by Donald A. Fischman was obtained from the Developmental Studies Hybridoma Bank developed under the auspices of the NICHD, National Institutes of Health and maintained by The University

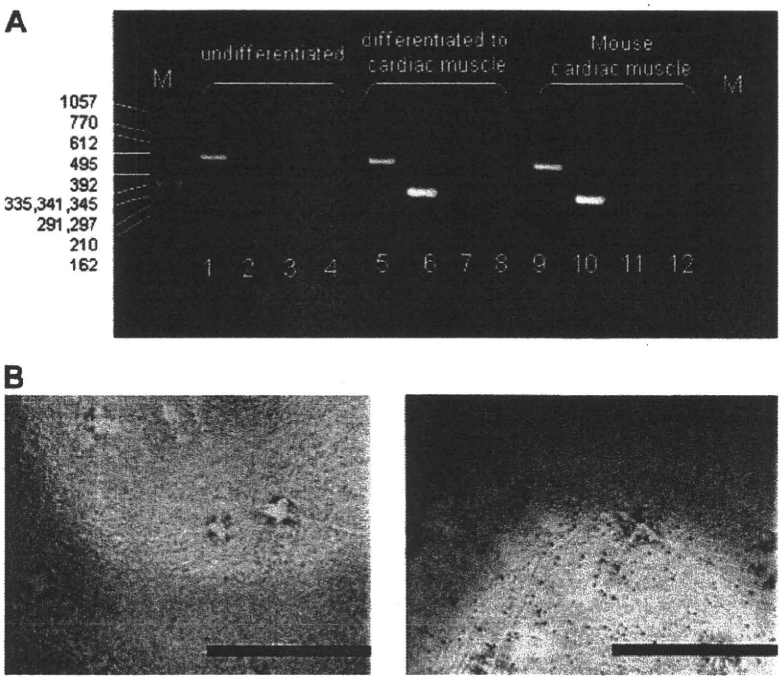

FIG. 2. **Differentiation of P19CL6 cells to cardiomyocytes in presence of DMSO.** *A*, RT-PCR analysis for the confirmation of cellular differentiation to cardiac muscle. *M*, DNA size marker (bp); *lanes 1*, *5*, and *9*, β-actin (503 bp), *lanes 2*, *6*, and *10*, α-cardiac myosin heavy chain (302 bp); *lanes 3*, *7*, and *11*, β-cardiac myosin heavy chain (205 bp); *lanes 4*, *8*, and *12*, embryonic skeletal muscle (151 bp). *B*, immunocytochemistry for the confirmation of P19CL6 cell differentiation to cardiac muscle. Primary antibody, MF20 (mouse monoclonal anti-sarcomere myosin); secondary antibody, HRP polymer-conjugated IgG; chromogenic substrate, diaminobenzidine. The *bar* represents 1.0 cm.

of Iowa, Department of Biological Sciences, Iowa City, IA.), which is a sarcomeric myosin-specific monoclonal antibody, overnight at 4 °C. They were then washed by PBS and incubated with HRP-labeled secondary antibody (Zymed Laboratories Inc.) for 10 min at room temperature. After washing, diaminobenzidine solution was added, and the reaction was stopped by washing with water. In the case of P19C6, anti-mouse neurofilament 160 was used as the primary antibody, and the other part of the procedure was performed similarly.

RESULTS

Concept—Our strategy of a glycoblotting-based rapid and quantitative glycomics designed for whole cellular *N*-glycans/free oligosaccharides using BlotGlyco (BlotGlyco H) beads is diagrammed in Fig. 1. The specific steps of this optimized protocol involve (i) enzymatic release of entire *N*-glycans from cellular glycoprotein fractions, including both cell surface and endogenous glycoproteins, (ii) glycoblotting (chemoselective enrichment) by BlotGlyco beads, (iii) on-bead derivatization and labeling with a reagent to enhance MS sensitivity by *trans*-iminization, and (iv) subsequent quantitative mass spectrometry-based glycomics and typing subgroups of characteristic glycoforms, namely glycotypes, in the presence of an internal standard. The key difference when compared with other published approaches for cellular glycomics is specific chemistry-based enrichment of entire *N*-glycans by a commercially available high density hydrazide bead (BlotGlyco) that allows for high throughput and quantitative glycan profiling. Through on-bead chemical protection of carboxyl groups, both human sialic acid Neu5Ac and non-human sialic acid Neu5Gc are stabilized to prevent the significant cleavage at the sensitive *O*-glycoside linkage of sialosides during the high energy ionization process in mass spectrometry. Given that human ESCs and iPS cells currently being developed are produced by using animal-derived materials such as serum and feeder layers or even fractionated glycoproteins, it is important to address potential contamination by introduction of non-human sialic acid Neu5Gc into human stem cell lines proposed for therapeutic applications in humans (13, 21). The reaction conditions and all procedures are carefully optimized by using not only mouse embryonic cells but also various human cancer cell lines to maximize efficacy of *N*-glycan enrichment and reproducibility of data acquisition. To facilitate quantitative *N*-glycan profiling analysis, the expression level of individual *N*-glycans was normalized and represented by using a standardized unit (pmol/200 μg of cellular proteins). We note that the present protocol is readily feasible for any type of mammalian cells, and the efficiency of glycoblotting is not dependent on cell type when the required cell numbers (for example, confluence on a 6-cm dish; ~5×10^6 cells) can be prepared. Rapid and quantitative analysis of major *N*-glycans (60–80 major glycoforms) enriched by the glycoblotting method provided us with reliable and satisfactory information for investigating structural changes in entire *N*-glycans and comparing the ratio of significant glycoforms by bar coding with characteristic subtypes, namely stage-specific embryonic glycotypes, during dynamic cell differentiation and proliferation.

Monitoring Entire N-Glycan Expression during Mouse P19 Cell Differentiations—Herein we selected the mouse P19 subclone to evaluate efficiency and versatility of our glycoblotting-based strategy. P19C6 cells are mouse embryonic car-

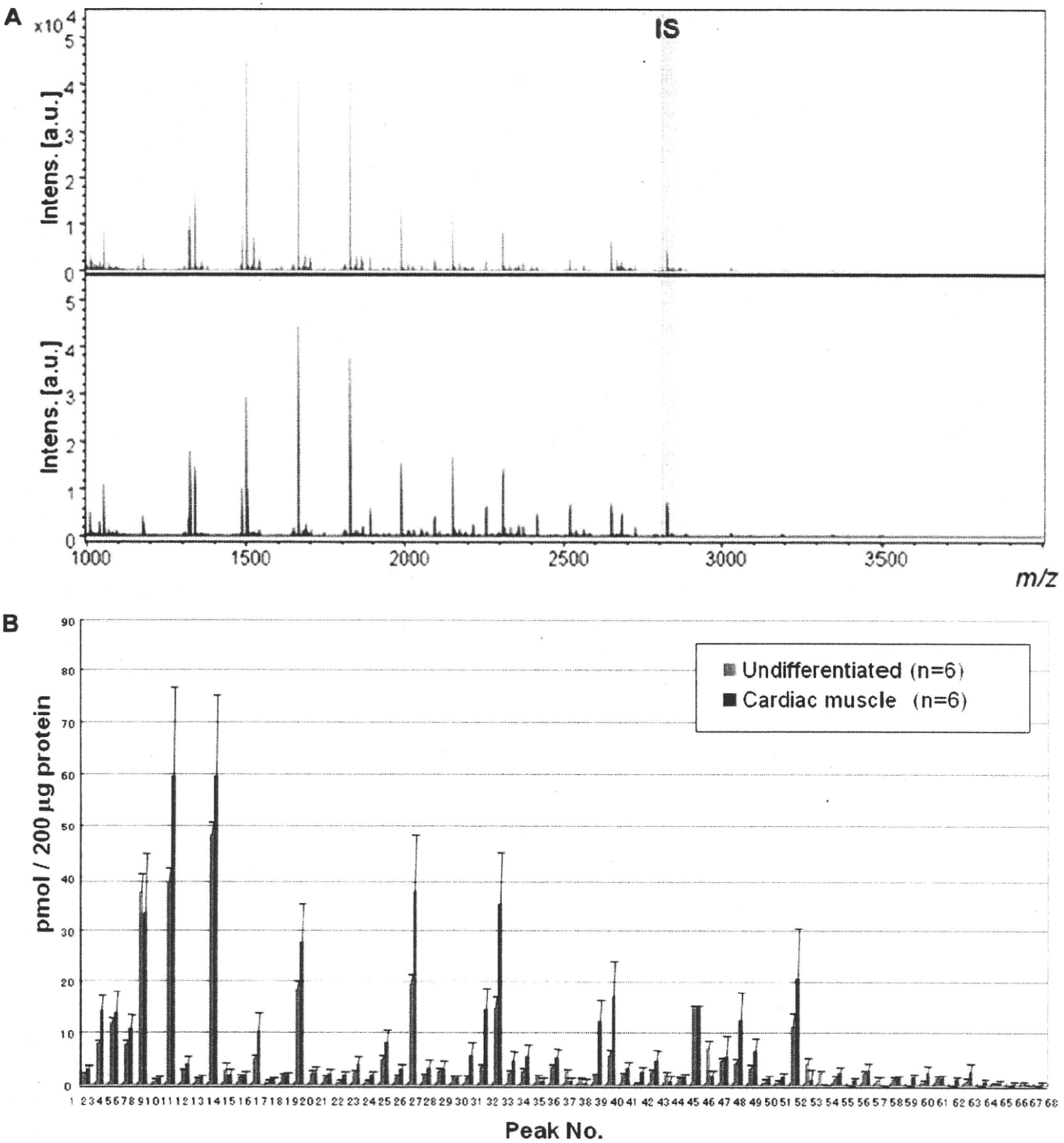

FIG. 3. **Large scale *N*-glycan analysis during P19CL6 cell differentiation.** *A*, MALDI-TOF-MS of whole *N*-glycans of undifferentiated and differentiated cells. *IS*, internal standard. *B*, quantitative and total glycomics of undifferentiated and differentiated cells. *C*, magnification to visualize increased glycans (*, $p < 0.01$; **, $p < 0.05$). *D*, magnification to visualize decreased glycans (*, $p < 0.01$; **, $p < 0.05$). Error bars mean standard deviations. *E*, bar coding analysis. *Intens.*, intensity; *a.u.*, arbitrary units.

cinoma cells and serve as a common model for studying neuronal differentiation after RA inducement (32). P19 cells treated with lower level RA or DMSO differentiate into muscle (33), and P19CL6 cells, a well established subclone derived from P19 cells, efficiently differentiate into beating cardiomyocytes by treatment with 1% DMSO (27, 34).

Differentiation of P19CL6 Cells to Cardiomyocytes—In the present study, we carefully characterized whole *N*-glycans of

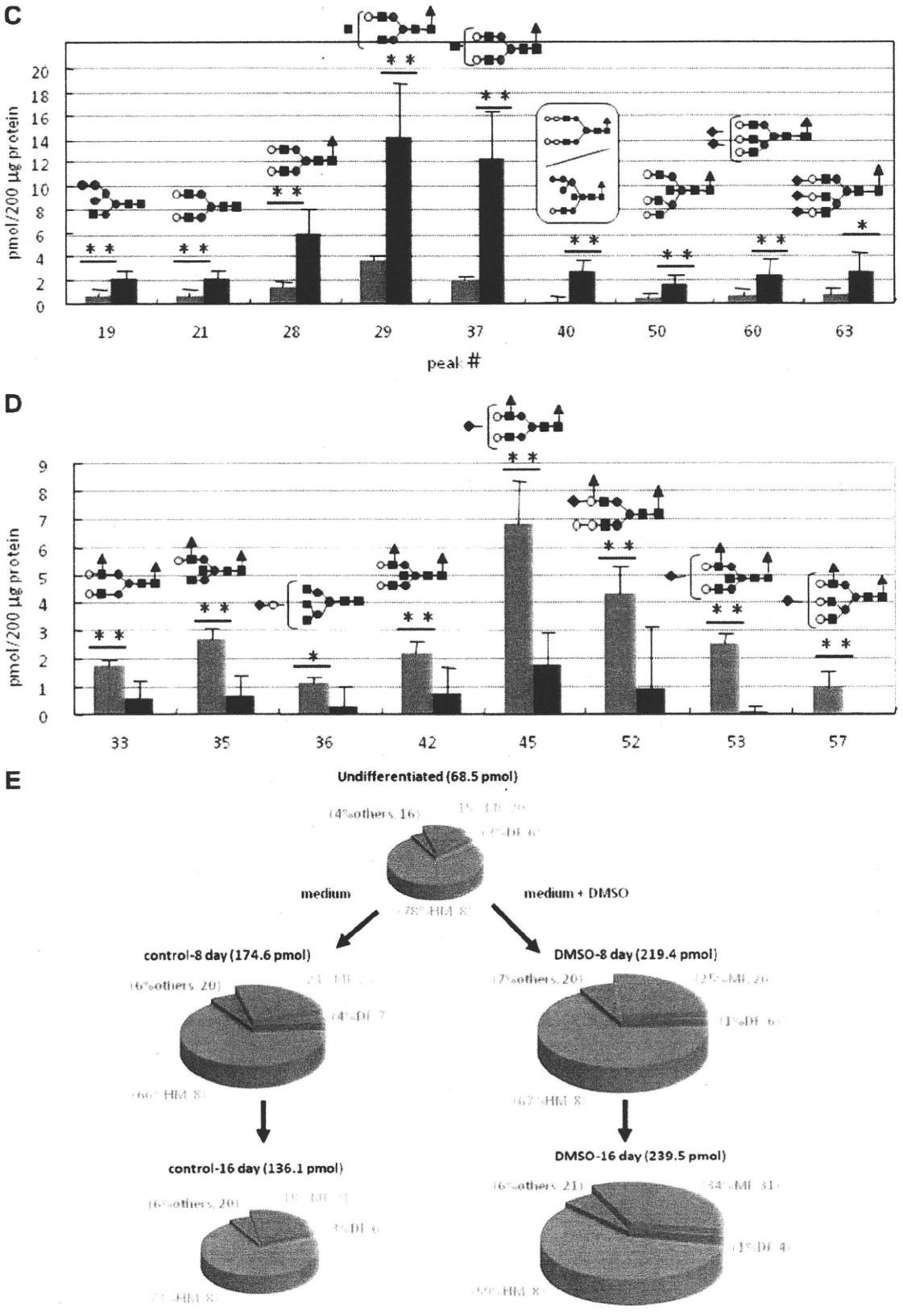

FIG. 3—*continued*

TABLE I
Glycoforms detected during P19CL6 cell differentiation
Hex, hexose; dHex, deoxyhexose; HexNAc, *N*-acetylhexosamine.

Peak no. CL6	*m/z*	Composition
1	1178.50	$Hex_2(HexNAc)_2$
2	1324.55	$Hex_2(HexNAc)_2dHex_1$
3	1340.55	$Hex_3(HexNAc)_2$
4	1486.61	$Hex_3(HexNAc)_2dHex_1$
5	1502.60	$Hex_4(HexNAc)_2$
6	1543.63	$Hex_3(HexNAc)_3$
7	1664.65	$Hex_5(HexNAc)_2$
8	1689.69	$Hex_3(HexNAc)_3dHex_1$
9	1746.71	$Hex_3(HexNAc)_4$
10	1826.71	$Hex_6(HexNAc)_2$
11	1848.74	$Hex_3(HexNAc)_4(NeuAc)_1$
12	1851.74	$Hex_4(HexNAc)_3dHex_1$
13	1892.76	$Hex_3(HexNAc)_4dHex_1$
14	1908.76	$Hex_4(HexNAc)_4$
15	1949.79	$Hex_3(HexNAc)_5$
16	1988.76	$Hex_7(HexNAc)_2$
17	2010.79	$Hex_4(HexNAc)_3(NeuAc)_1$
18	2013.79	$Hex_5(HexNAc)_3dHex_1$
19	2029.79	$Hex_6(HexNAc)_3(NeuAc)_1$
20	2054.82	$Hex_4(HexNAc)_4dHex_1$
21	2070.81	$Hex_5(HexNAc)_4$
22	2095.84	$Hex_3(HexNAc)_5dHex_1$
23	2111.84	$Hex_4(HexNAc)_5$
24	2150.81	$Hex_8(HexNAc)_2$
25	2156.85	$Hex_4(HexNAc)_3dHex_1(NeuAc)_1$
26	2172.84	$Hex_5(HexNAc)_3(NeuAc)_1$
27	2213.87	$Hex_4(HexNAc)_4(NeuAc)_1$
28	2216.87	$Hex_5(HexNAc)_4dHex_1$
29	2257.90	$Hex_4(HexNAc)_5dHex_1$
30	2312.86	$Hex_9(HexNAc)_2$
31	2334.90	$Hex_6(HexNAc)_3(NeuAc)_1$
32	2359.93	$Hex_4(HexNAc)_4dHex1(NeuAc)_1$
33	2362.93	$Hex_5(HexNAc)_4dHex_2$
34	2375.92	$Hex_5(HexNAc)_4(NeuAc)_1$
35	2403.95	$Hex_4(HexNAc)_5dHex_2$
36	2416.95	$Hex_4(HexNAc)_6(NeuAc)_1$
37	2419.95	$Hex_5(HexNAc)_5dHex_1$
38	2521.98	$Hex_5(HexNAc)_4dHex_1(NeuAc)_1$
39	2537.98	$Hex_6(HexNAc)_4(NeuAc)_1$
40	2540.98	$Hex_7(HexNAc)_5dHex_1$
41	2563.01	$Hex_4(HexNAc)_5dHex_1(NeuAc)_1$
42	2566.01	$Hex_5(HexNAc)_5dHex_2$
43	2579.00	$Hex_5(HexNAc)_5(NeuAc)_1$
44	2651.33	Internal standard
45	2668.04	$Hex_5(HexNAc)_4dHex_2(NeuAc)_1$
46	2681.03	$Hex_5(HexNAc)_4(NeuAc)_2$
47	2684.03	$Hex_6(HexNAc)_4dHex_1(NeuAc)_1$
48	2725.06	$Hex_5(HexNAc)_5dHex_1(NeuAc)_1$
49	2741.06	$Hex_6(HexNAc)_6(NeuAc)_1$
50	2785.08	$Hex_6(HexNAc)_6dHex_1$
51	2827.09	$Hex_5(HexNAc)_4dHex_1(NeuAc)_2$
52	2830.09	$Hex_6(HexNAc)_4dHex_2(NeuAc)_1$
53	2871.12	$Hex_5(HexNAc)_5dHex_2(NeuAc)_1$
54	2887.11	$Hex_6(HexNAc)_5dHex_1(NeuAc)_1$
55	2928.14	$Hex_5(HexNAc)_6dHex_1(NeuAc)_1$
56	3030.17	$Hex_5(HexNAc)_5dHex_1(NeuAc)_2$
57	3033.17	$Hex_6(HexNAc)_5dHex_2(NeuAc)_1$
58	3046.17	$Hex_6(HexNAc)_5(NeuAc)_2$
59	3090.19	$Hex_6(HexNAc)_6dHex_1(NeuAc)_1$
60	3192.22	$Hex_6(HexNAc)_5dHex_1(NeuAc)_2$
61	3351.28	$Hex_6(HexNAc)_5(NeuAc)_3$
62	3395.30	$Hex_6(HexNAc)_6dHex_1(NeuAc)_2$
63	3497.34	$Hex_6(HexNAc)_5dHex_1(NeuAc)_3$
64	3557.36	$Hex_7(HexNAc)_6dHex_1(NeuAc)_2$
65	3700.42	$Hex_6(HexNAc)_6dHex_1(NeuAc)_3$
66	3862.47	$Hex_7(HexNAc)_6dHex_1(NeuAc)_3$
67	4021.52	$Hex_7(HexNAc)_6(NeuAc)_4$
68	4167.58	$Hex_7(HexNAc)_6dHex_1(NeuAc)_4$

P19C6 cells with or without inducement into neural cells as well P19CL6 cells differentiated into cardiomyocytes. After 1% DMSO treatment, P19CL6 cells formed a monolayer at day 3 and multilayers on day 5 and started beating synchronously at day 16 of differentiation as reported (27), whereas control cells did not show any changes at the same period of culture. The differentiation into cardiac muscle was confirmed by conventional RT-PCR detecting mRNA coding cardiomyocyte-specific proteins and immunocytochemistry (Fig. 2, *A* and *B*). As shown in Fig. 2*A*, α- and β-cardiac myosin heavy chains, the markers of cardiomyocytes (35), were specifically detected in the DMSO-treated 16-day cultured P16CL6 cells and mouse cardiac muscles as a positive control. In addition, mouse monoclonal antibody MF20 reacted specifically with differentiated cardiomyocytes (Fig. 2*B*), indicating that differentiated cells readily express sarcomeric myosin.

Whole *N*-glycans of P19CL6 cells (undifferentiated cells) and differentiated cells on day 18 ($n = 6$, six dishes each for both cells) were analyzed and identified for the first time by means of glycoblotting-based high throughput MALDI-TOF mass spectrometry (Fig. 3*A*). As summarized in Table I, 67 kinds of glycoforms were detected and quantified reproducibly in both cases. When the full portraits of *N*-glycan diversity of both cells were represented quantitatively (Fig. 3*B*), it seems likely that high mannose type *N*-glycans (peak numbers 1(M2), 3(M3), 5(M4), 7(M5), 10(M6), 16(M7), 24(M8), and 30(M9)) are major components throughout cardiomyocytic differentiation. However, it was also clearly suggested that expression levels of 26 *N*-glycans were significantly accompanied by cellular differentiation; 19 *N*-glycans, most of which are monofucosylated glycoforms, were increased concertedly, whereas seven difucosylated *N*-glycans decreased. Changes in two glycoforms (peak numbers 40 and 53) were especially significant ($p < 0.001$); their expression level was increased 16-fold (peak number 40) and decreased 30-fold (peak number 53) according to differentiation, respectively. Fig. 3, *C* and *D*, highlights dramatically changed *N*-glycan structures during cell differentiation; namely monofucosylated *N*-glycans were drastically increased, whereas difucosylated *N*-glycans decreased in comparison with the expression level of whole cellular *N*-glycans.

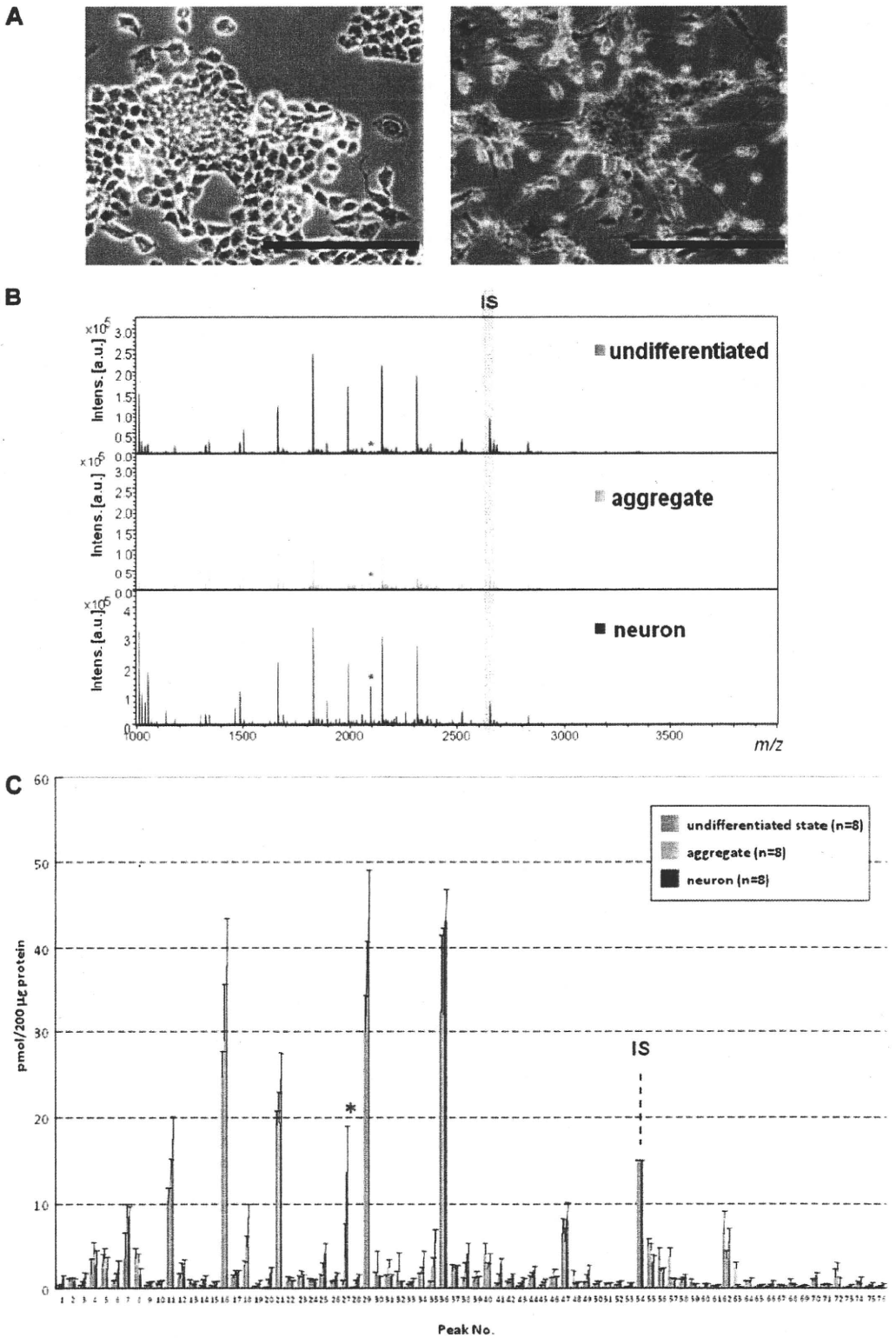

FIG. 4. **Differentiation of P19C6 cells to neural cells.** *A*, immunocytochemistry for the confirmation of neural differentiation. Primary antibody, mouse monoclonal anti-neurofilament 160; secondary antibody, HRP polymer-conjugated IgG; chromogenic substrate, diaminobenzidine. The *bar* represents 200 μm. *B*, MALDI-TOF-MS of whole *N*-glycans of undifferentiated and differentiated cells. *IS*, internal standard. * represents peak number 27. *C*, quantitative and total glycomics of undifferentiated and differentiated cells. *IS*, internal standard. * represents peak number 27. *D*, magnification to visualize increased glycans. *E*, bar coding analysis.

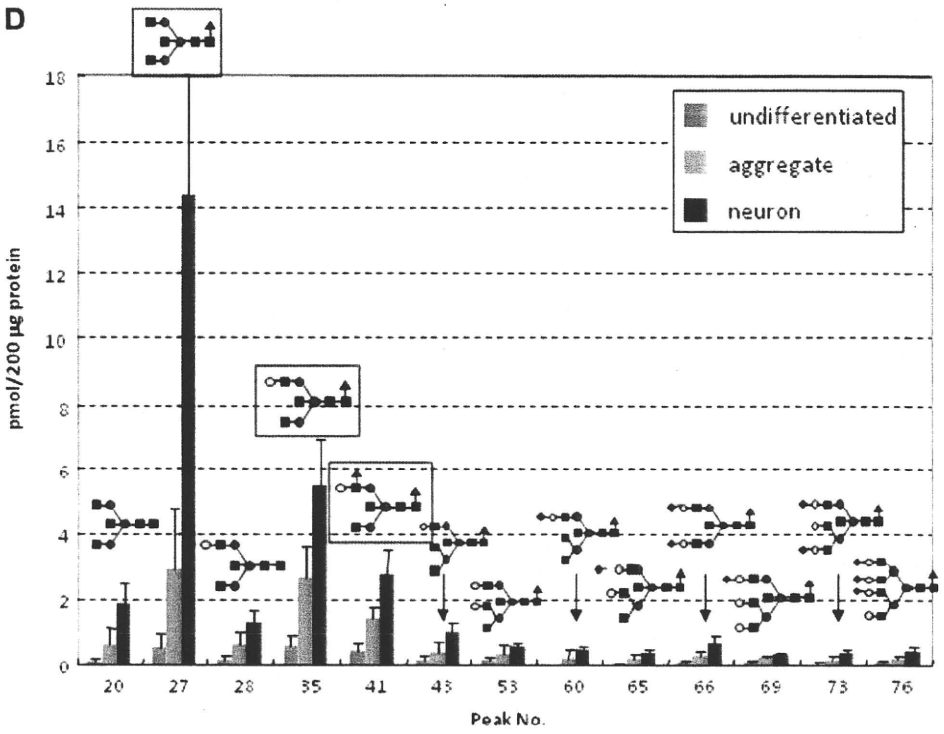

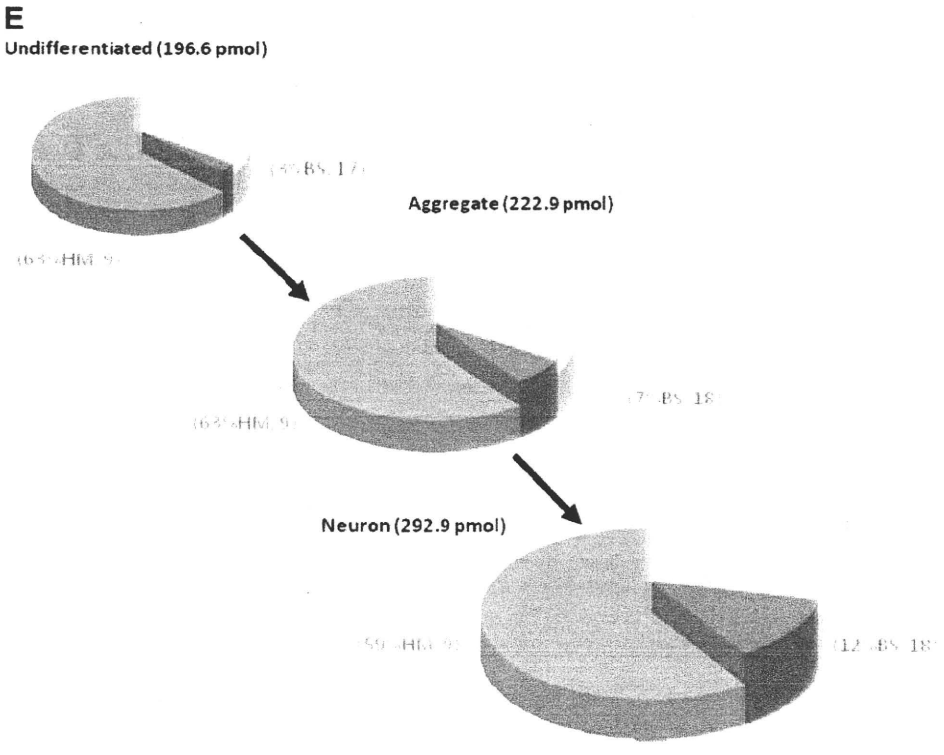

FIG. 4—*continued*

The significance of the dramatic changes in the expression level of two distinct glycotypes uncovered by quantitative glycomics of entire cellular *N*-glycans was revealed much more simply by bar coding individual glycotypes such as high mannose type (HM), monofucosylated type (MF), difucosylated type (DF), and others (O) (Fig. 3*E*). It is clear that the total *N*-glycan expression level was significantly increased from undifferentiated (68.5 pmol/200 μg of protein) to the interme-

TABLE II
Glycoforms detected during P19C6 cell differentiation
Hex, hexose; dHex, deoxyhexose; HexNAc, *N*-acetylhexosamine.

Peak no.	*m/z*	Composition
1	1137.47	$Hex_3(HexNAc)_1$
2	1178.50	$Hex_2(HexNAc)_2$
3	1299.52	$Hex_4(HexNAc)_1$
4	1324.55	$Hex_2(HexNAc)_2dHex_1$
5	1340.55	$Hex_3(HexNAc)_2$
6	1461.57	$Hex_5(HexNAc)_1$
7	1486.61	$Hex_3(HexNAc)_2dHex_1$
8	1502.60	$Hex_4(HexNAc)_2$
9	1543.63	$Hex_3(HexNAc)_3$
10	1623.63	$Hex_6(HexNAc)_1$
11	1664.65	$Hex_5(HexNAc)_2$
12	1689.69	$Hex_3(HexNAc)_3dHex_1$
13	1705.68	$Hex_4(HexNAc)_3$
14	1746.71	$Hex_3(HexNAc)_4$
15	1785.68	$Hex_7(HexNAc)_1$
16	1826.71	$Hex_6(HexNAc)_2$
17	1851.74	$Hex_4(HexNAc)_3dHex_1$
18	1892.76	$Hex_3(HexNAc)_4dHex_1$
19	1908.76	$Hex_4(HexNAc)_4$
20	1949.79	$Hex_3(HexNAc)_5$
21	1988.76	$Hex_7(HexNAc)_2$
22	2010.79	$Hex_4(HexNAc)_3(NeuAc)_1$
23	2013.79	$Hex_5(HexNAc)_3dHex_1$
24	2029.79	$Hex_6(HexNAc)_3(NeuAc)_1$
25	2054.82	$Hex_4(HexNAc)_4dHex_1$
26	2070.81	$Hex_5(HexNAc)_4$
27	2095.84	$Hex_3(HexNAc)_5dHex_1$
28	2111.84	$Hex_4(HexNAc)_5$
29	2150.81	$Hex_8(HexNAc)_2$
30	2172.84	$Hex_5(HexNAc)_3(NeuAc)_1$
31	2175.84	$Hex_6(HexNAc)_3dHex_1$
32	2200.88	$Hex_4(HexNAc)_4dHex_2$
33	2213.87	$Hex_4(HexNAc)_4(NeuAc)_1$
34	2216.87	$Hex_5(HexNAc)_4dHex_1$
35	2257.90	$Hex_4(HexNAc)_5dHex_1$
36	2312.86	$Hex_9(HexNAc)_2$
37	2334.90	$Hex_6(HexNAc)_3(NeuAc)_1$
38	2359.93	$Hex_4(HexNAc)_4dHex_1(NeuAc)_1$
39	2362.93	$Hex_5(HexNAc)_4dHex_2$
40	2375.92	$Hex_5(HexNAc)_4(NeuAc)_1$
41	2403.95	$Hex_4(HexNAc)_5dHex_2$
42	2419.95	$Hex_5(HexNAc)_5dHex_1$
43	2460.98	$Hex_4(HexNAc)_6dHex_1$
44	2474.92	$Hex_{10}(HexNAc)_2$
45	2480.95	$Hex_6(HexNAc)_3dHex_1(NeuAc)_1$
46	2508.99	$Hex_5(HexNAc)_4dHex_3$
47	2521.98	$Hex_5(HexNAc)_4dHex_1(NeuAc)_1$
48	2537.98	$Hex_6(HexNAc)_4(NeuAc)_1$
49	2563.01	$Hex_4(HexNAc)_5dHex_1(NeuAc)_1$
50	2566.01	$Hex_5(HexNAc)_5dHex_2$
51	2579.00	$Hex_5(HexNAc)_5(NeuAc)_1$
52	2582.00	$Hex_6(HexNAc)_5dHex_1$
53	2623.03	$Hex_5(HexNAc)_6dHex_1$
54	2651.33	Internal standard
55	2668.04	$Hex_5(HexNAc)_4dHex_2(NeuAc)_1$
56	2681.03	$Hex_5(HexNAc)_4(NeuAc)_2$
57	2684.03	$Hex_6(HexNAc)_4dHex_1(NeuAc)_1$
58	2725.06	$Hex_5(HexNAc)_5dHex_1(NeuAc)_1$
59	2741.06	$Hex_6(HexNAc)_6(NeuAc)_1$
60	2766.09	$Hex_4(HexNAc)_6dHex_1(NeuAc)_1$
61	2785.08	$Hex_6(HexNAc)_6dHex_1$
62	2827.09	$Hex_5(HexNAc)_4dHex_1(NeuAc)_2$
63	2830.09	$Hex_6(HexNAc)_4dHex_2(NeuAc)_1$
64	2887.11	$Hex_6(HexNAc)_5dHex_1(NeuAc)_1$
65	2928.14	$Hex_5(HexNAc)_6dHex_1(NeuAc)_1$
66	3030.17	$Hex_5(HexNAc)_5dHex_1(NeuAc)_2$
67	3033.17	$Hex_6(HexNAc)_5dHex_2(NeuAc)_1$
68	3046.17	$Hex_6(HexNAc)_5(NeuAc)_2$
69	3090.19	$Hex_6(HexNAc)_6dHex_1(NeuAc)_1$
70	3192.22	$Hex_6(HexNAc)_5dHex_1(NeuAc)_2$
71	3338.28	$Hex_6(HexNAc)_5dHex2(NeuAc)_2$
72	3351.28	$Hex_6(HexNAc)_5(NeuAc)_3$
73	3395.30	$Hex_6(HexNAc)_6dHex_1(NeuAc)_2$
74	3497.34	$Hex_6(HexNAc)_5dHex_1(NeuAc)_3$
75	3557.36	$Hex_7(HexNAc)_6dHex_1(NeuAc)_2$
76	3862.47	$Hex_7(HexNAc)_6dHex_1(NeuAc)_3$

diate cells at day 8 (219.4 pmol/200 μg of protein) and differentiated cells at day 16 (239.5 pmol/200 μg of protein). It was revealed that the ratio of glycotype MF was increased from 15 to 34%, and at least 11 glycoforms could be assigned as newly generated *N*-glycans involved in the glycotype MF after differentiation, whereas the others, glycotype HM, glycotype DF, and glycotype O, showed no significant change both in the ratio and the number of glycoforms. When P19CL6 cells were subjected to culture continuously until day 16 without DMSO induction, there was no notable change in entire *N*-glycan expression during this period. Surprisingly, these cells exhibited *N*-glycan profiles quite similar to each other in terms of not only the ratio of the above four glycotypes but also the numbers of glycoforms identified in the individual glycotypes.

Differentiation of P19C6 Cells and ESCs to Neural Cells—Versatility of the present concept and protocol was demonstrated by using P19C6 cells that differentiate into neural cells by RA inducement in which differentiation can be confirmed conventionally by immunocytochemistry using mouse monoclonal antibody (anti-neurofilament 160 monoclonal antibody) as shown in Fig. 4*A*. Fig. 4*B* shows MALDI-TOF mass spectra of whole *N*-glycans enriched by glycoblotting at three distinct stages observed during P19C6 cell differentiation to neural cells, namely undifferentiated, aggregate (day 4), and differentiated neural cells (day 9). A total of 75 *N*-glycans were identified; they are summarized in Table II and represented in a quantitative manner in Fig. 4*C*. In the case of P19C6 cell differentiation into neural cells, it was revealed that 12 glycoforms (peak numbers 20, 27, 28, 35, 41, 43, 53, 60, 65, 66, 69, and 73) were identified as bisect type (BS) *N*-glycans among 13 *N*-glycans that increased more than 5-fold after differentiation (Fig. 4*D*). The merit of bar coding analysis based on the characteristic subtypes is clear because profiling by focusing on glycotype BS clearly shows a drastic increase of this subtype (from 3 to 12%) compared with glycotype HM (from

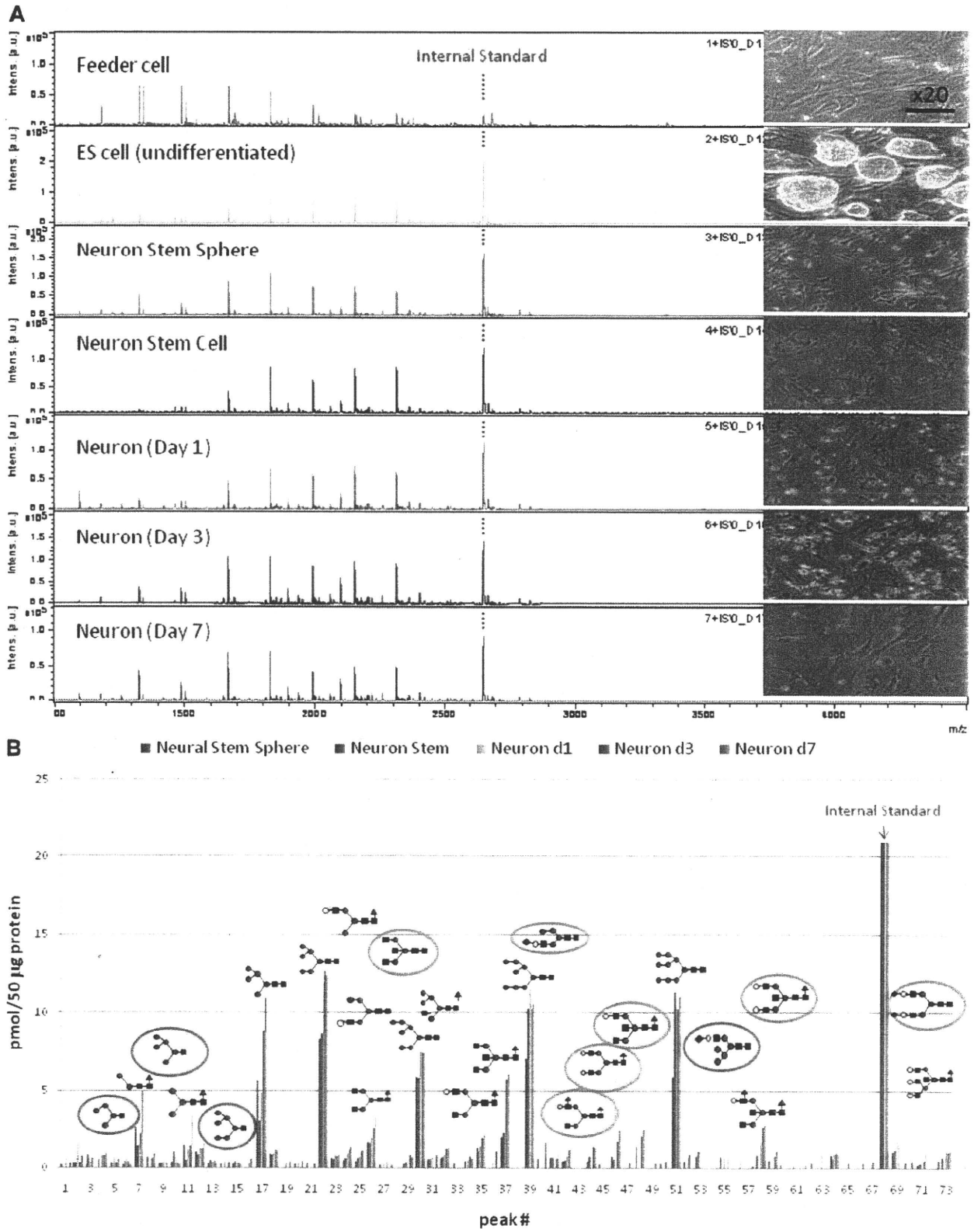

FIG. 5. **Differentiation of mouse ESCs to neural cells.** *A*, MALDI-TOF-MS spectra during cell differentiation. *B*, quantitative glycan profiling during ESC differentiation. *C*, bar coding analysis. *D*, novel glycan biomarkers for identifying and monitoring the processes of mouse neural cell differentiation. *Intens.*, intensity; *a.u.*, arbitrary units; *d*, day.

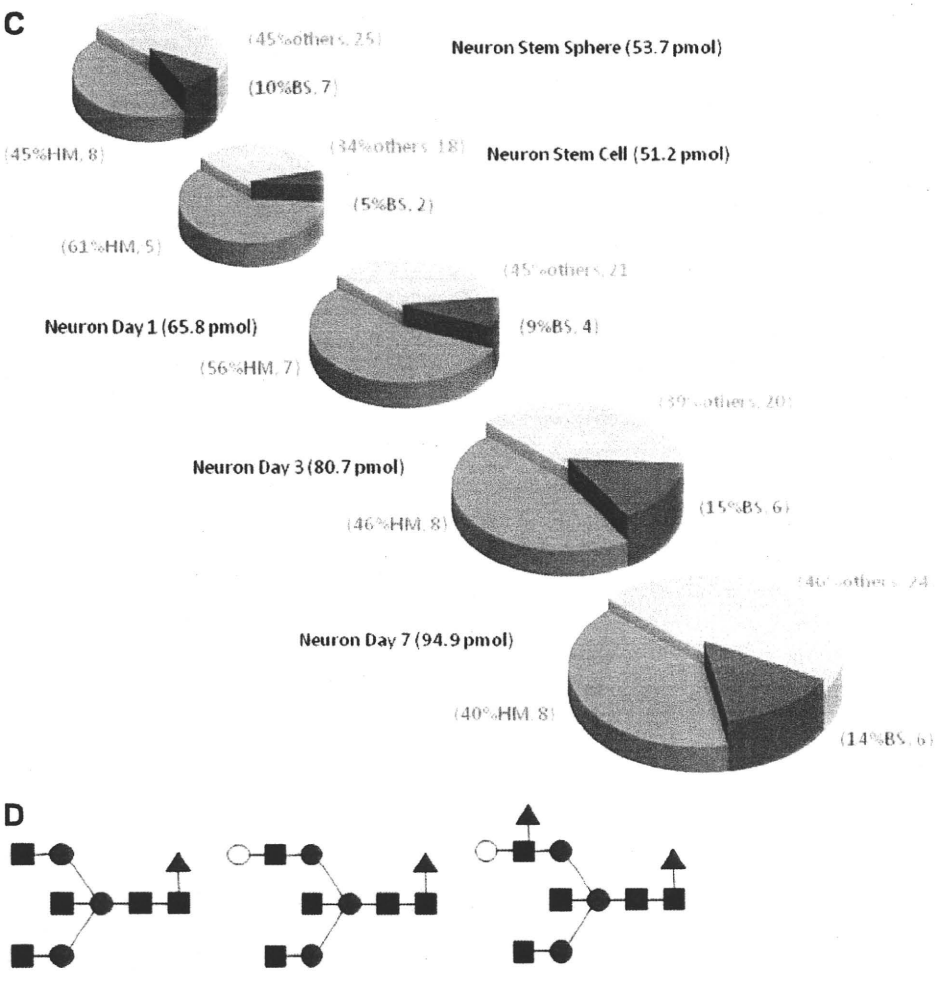

FIG. 5—*continued*

63 to 59%) and glycotype O (from 34 to 29%) (Fig. 4*E*). On the contrary, L-fucose-focused bar coding analysis used in the case of the P19CL6/cardiomyocytes system did not show any meaningful *N*-glycans expression change during differentiation: glycotype HM, from 63 to 59%; glycotype DF, from 6 to 4%; glycotype MF, from 21 to 30%; and glycotype O, from 10 to 7%.

Our interest was next directed toward alteration of *N*-glycan expression of mouse ESC differentiation to neural cells. We considered that neural cells differentiated from mouse ESCs should also exhibit a structural alteration in the stage-specific glycotypes, an increase of glycotype BS, similar to those observed in P19C6 cell differentiation. Fig. 5, *A* and *B*, and Table III show the results of MALDI-TOF-MS of all typical cellular stages during mouse ESC differentiation into neural cells. As expected, bar coding analysis by three glycotypes used in the P19C6 cells demonstrated the significant increase of glycotype BS (10% at neural stem sphere or 5% at neural stem cell to 14% at neural cell day 7) in comparison with glycotype HM (45% at neural stem sphere or 61% at neural stem cell to 40%) and glycotype O (45% at neural stem sphere or 34% at neural stem cell to 46%) (Fig. 5*C*). During the differentiation from neural stem sphere into neural stem cells, it seems likely that an increase of glycotype HM (from 45 to 61%) and a decrease of glycotype BS (from 10 to 5%) occurred concurrently, although the reason is not clear. Surprisingly, it was revealed that neural cells differentiated from ESCs also exhibited up-regulated high level expression of the same three glycoforms (Fig. 5*D*; peak numbers 37, 48, and 58 in Fig. 5*B*) as those observed in P19C6 differentiation (peak numbers 27, 35, and 41 in Fig. 4*D*). We could not detect any Neu5Gc residue in whole *N*-glycans identified in the present study, and the expression levels of any *N*-glycans containing Neu5Ac residue(s) did not accompany P19 series cell differentiation. This means that bar coding analysis focusing on the expression level of Neu5Ac did not work for identifying stage-specific embryonic glycotypes in these cell lines. Our preliminary result (n = 3) indicates clearly the importance of the stage-specific embryonic glycotype BS as a new class of biomarkers for identifying and monitoring processes of mouse ESC differentiation into neural cells, although the effect of feeder cells and other various factors

TABLE III
Glycoforms detected during ESC differentiation
Hex, hexose; dHex, deoxyhexose; HexNAc, *N*-acetylhexosamine.

Peak no. ESC	*m/z*	Composition
1	934.39	Hex_3
2	1096.44	Hex_4
3	1137.47	$Hex_3(HexNAc)_1$
4	1178.50	$Hex_2(HexNAc)_2$
5	1258.49	Hex_5
6	1299.52	$Hex_4(HexNAc)_1$
7	1324.55	$Hex_2(HexNAc)_2dHex_1$
8	1340.55	$Hex_3(HexNAc)_2$
9	1420.55	Hex_6
10	1461.57	$Hex_5(HexNAc)_1$
11	1486.61	$Hex_3(HexNAc)_2dHex_1$
12	1502.60	$Hex_4(HexNAc)_2$
13	1543.63	$Hex_3(HexNAc)_3$
14	1582.60	Hex_7
15	1623.63	$Hex_6(HexNAc)_1$
16	1645.66	$Hex_2(HexNAc)_2dHex_1$
17	1664.65	$Hex_5(HexNAc)_2$
18	1689.69	$Hex_3(HexNAc)_3dHex_1$
19	1705.68	$Hex_4(HexNAc)_3$
20	1746.71	$Hex_3(HexNAc)_4$
21	1785.68	$Hex_7(HexNAc)_1$
22	1826.71	$Hex_6(HexNAc)_2$
23	1848.74	$Hex_3(HexNAc)_3(NeuAc)_1$
24	1851.74	$Hex_4(HexNAc)_3dHex_1$
25	1867.73	$Hex_5(HexNAc)_3$
26	1892.76	$Hex_3(HexNAc)_4dHex_1$
27	1908.76	$Hex_4(HexNAc)_4$
28	1947.73	$Hex_8(HexNAc)_1$
29	1949.79	$Hex_3(HexNAc)_5$
30	1988.76	$Hex_7(HexNAc)_2$
31	2010.79	$Hex_4(HexNAc)_3(NeuAc)_1$
32	2013.79	$Hex_5(HexNAc)_3dHex_1$
33	2029.79	$Hex_6(HexNAc)_3$
35	2054.82	$Hex_4(HexNAc)_4dHex_1$
36	2070.81	$Hex_5(HexNAc)_4$
37	2095.84	$Hex_3(HexNAc)_5dHex_1$
38	2111.84	$Hex_4(HexNAc)_5$
39	2150.81	$Hex_8(HexNAc)_2$
40	2156.85	$Hex_4(HexNAc)_3dHex_1(NeuAc)_1$
41	2172.84	$Hex_5(HexNAc)_3(NeuAc)_1$
42	2175.84	$Hex_6(HexNAc)_3dHex_1$
43	2191.84	$Hex_7(HexNAc)_3$
44	2200.88	$Hex_4(HexNAc)_4dHex_2$
45	2213.87	$Hex_4(HexNAc)_4(NeuAc)_1$
46	2216.87	$Hex_5(HexNAc)_4dHex_1$
47	2232.92	$Hex_6(HexNAc)_4$
48	2257.90	$Hex_4(HexNAc)_5dHex_1$
49	2273.90	$Hex_5(HexNAc)_5$
50	2298.92	$Hex_3(HexNAc)_6dHex_1$
51	2312.86	$Hex_9(HexNAc)_2$
52	2318.90	$Hex_5(HexNAc)_3dHex_1(NeuAc)_1$
53	2334.90	$Hex_6(HexNAc)_3(NeuAc)_1$
54	2359.93	$Hex_4(HexNAc)_4dHex_1(NeuAc)_1$
55	2375.92	$Hex_5(HexNAc)_4(NeuAc)_1$
56	2378.92	$Hex_6(HexNAc)_4dHex_1$
57	2394.92	$Hex_7(HexNAc)_4$
58	2403.95	$Hex_4(HexNAc)_5dHex_2$
59	2419.95	$Hex_5(HexNAc)_5dHex_1$
60	2460.98	$Hex_4(HexNAc)_6dHex_1$
61	2474.92	$Hex_{10}(HexNAc)_2$
62	2480.95	$Hex_6(HexNAc)_3dHex_1(NeuAc)_1$
63	2508.99	$Hex_5(HexNAc)_4dHex_3$
64	2521.98	$Hex_5(HexNAc)_4dHex_1(NeuAc)_1$
65	2537.98	$Hex_6(HexNAc)_4(NeuAc)_1$
66	2540.98	$Hex_7(HexNAc)_5dHex_1$
67	2566.01	$Hex_5(HexNAc)_5dHex_2$
68	2651.33	Internal standard
69	2668.04	$Hex_5(HexNAc)_4dHex_2(NeuAc)_1$
70	2681.03	$Hex_5(HexNAc)_4(NeuAc)_2$
71	2684.03	$Hex_6(HexNAc)_4dHex_1(NeuAc)_1$
72	2712.79	$Hex_5(HexNAc)_4(NeuGc)_2$
73	2827.09	$Hex_5(HexNAc)_4dHex_1(NeuAc)_2$

of individual culture conditions used on the ratio of these glycotypes must be examined carefully.

DISCUSSION

For most mammalian cell types, it is not known which proteins are expressed at each cellular stage and how these protein expression patterns change quantitatively upon differentiation and proliferation. Flow cytometry and immunohistochemistry have been generally used for the identification of cell surface proteins such as cell differentiation markers. However, it is not currently possible to profile a global view of the cell surface protein landscape due to the limitation of feasible antibodies with validated specificity and affinity strength and the difficulty in the development of multiplexed assays for identifying sets of cell surface proteins in a single experiment.

Large scale proteomics analysis by two-dimensional gel electrophoresis MALDI-TOF-MS suggested that only 17 proteins (0.7% of total detected ~2200 proteins) with different expression patterns may be involved in the DMSO-induced cardiac differentiation of P19CL6 cells (36). They also reported that real time PCR data showed discrepancies from that of proteomics in at least three kinds of proteins that reflected the importance of posttranslational modifications in expressed proteins. On the other hand, it was also reported that only 0.8% of total detected proteins (28 proteins of ~3500 proteins) were increased or decreased during the 8-day differentiation of P19 cells to neural cells (34, 37). Consequently, it was concluded that changes in the expression level of detected proteins are not helpful for identifying or monitoring the processes of cellular differentiation of both P19 and P19C6 cells. Compared with the results of proteome-based analysis, the high potential of the glycome-based approach is clear because our results revealed for the first time that 28% of glycoforms (19 *N*-glycans of 67 total *N*-glycans; peak numbers 13, 20, 21, 22, 25, 28, 29, 32, 34, 37, 38, 39, 40, 41, 47, 48, 54, 60, and 63) were increased, and 10% (7 of 67) were decreased during P19CL6 cell differentiation to car-

diomyocytes. Furthermore, the expression level of 31 *N*-glycans involved in the glycotype MF was up-regulated to 34% (78.2 pmol/200 μg of protein) against total detected *N*-glycan expression (239.5 pmol/200 μg of protein), whereas undifferentiated cells expressed only 15% glycotype MF (20 glycoforms). Interestingly, differentiated cardiomyocytes lost most Lewis X trisaccharide (SSEA-1) and sialyl-Lewis X tetrasaccharide moieties in major *N*-glycans as shown in Fig. 3*C*, whereas monofucosylation occurred specifically in the above 31 glycoforms at the GlcNAc residue involved in core chitobiose moiety after differentiation, suggesting that loss of cell adhesion through the interaction with selectins may be key to the differentiation of P19CL6 cells toward cardiomyocytes. It was also demonstrated that both P19C6 cells and ESCs showed quite similar drastic changes in the profiles of entire *N*-glycan expression during cell differentiation into neural cells in which the expression level of glycotype BS was up-regulated to 12 and 14% from 3 and 5%, respectively. Among *N*-glycans involved in the glycotype BS, three common bisect type glycoforms detected in neural cells were found to become new potential markers to identify and monitor the process of mouse neural cell differentiation. Given that the glycoforms corresponding to these three bisect type *N*-glycans have been known to exist in the mouse brain system (38, 39), this drastic up-regulation of the *N*-glycans involved in glycotype BS seems to be crucial for the differentiation to neural cells. Actually, GlcNAc-transferase III (*Mgat3* gene), a glycosyltransferase responsible for the synthesis of bisecting GlcNAc linkage, appears to be normally expressed at high levels in mammalian brain and kidney tissues (40, 41). However, the relationship between threshold in the expression level of glycotype BS and mechanism in P19C6 cell differentiation remains unclear.

In the present study, we demonstrated the versatility of glycoblotting-based quantitative glycomics in the investigation of dynamic glycoform alteration during mammalian cell proliferation and differentiation. A full portrait of *N*-glycan expression at each cell stage allowed identification of the characteristic glycotypes showing drastic and concerted expression changes during cell differentiation, termed stage-specific embryonic glycotypes. The present results indicate the existence of a threshold in expression level of the characteristic glycotypes required for initiating individual cell differentiations, although functional roles, mechanism, and designated partner molecules remain unknown. A microarray displaying major glycotypes expressed at individual cell stages should be a useful tool to elicit candidate partner molecules as well as the adhesion mechanism of the differentiated cells. However, we consider that most glycoproteins at the specific cell stage might share some biosynthetic pathways at the Golgi, resulting in the dynamic and large scale expression changes of glycotypes during cell differentiation. We should set a goal to compare and accumulate a database of whole *N*-glycan expression levels of feasible human ESC and iPS cell lines established by different laboratories and to make these resources readily available to the scientific community as soon as possible.

* This work was supported in part by a grant for "Innovative program for future drug discovery and medical care" from the Japan Science and Technology Agency and the Ministry of Education, Culture, Science, Sports, and Technology of Japan.

‖ To whom correspondence should be addressed. E-mail: shin@glyco.sci.hokudai.ac.jp.

REFERENCES

1. Stanton, L. W., and Bakre, M. M. (2007) Genomic and proteomic characterization of embryonic stem cells. *Curr. Opin. Chem. Biol.* **11,** 399–404
2. Kuramitsu, Y., and Nakamura, K. (2006) Proteomic analysis of cancer tissues: shedding light on carcinogenesis and possible biomarkers. *Proteomics* **6,** 5650–5661
3. Gonnet, F., Bouazza, B., Millot, G. A., Ziaei, S., Garcia, L., Butler-Browne, G. S., Mouly, V., Tortajada, J., Danos, O., and Svinartchouk, F. (2008) Proteome analysis of differentiating human myoblasts by dialysis-assisted two-dimensional gel electrophoresis (DAGE). *Proteomics* **8,** 264–278
4. Watkins, J., Basu, S., and Bogenhagen, D. F. (2008) A quantitative proteomic analysis of mitochondrial participation in p19 cell neuronal differentiation. *J. Proteome Res.* **7,** 328–338
5. Loring, J. F., and Rao, M. S. (2006) Establishing standards for the characterization of human embryonic stem cell lines. *Stem Cells* **24,** 145–150
6. Varki, A. (1993) Biological roles of oligosaccharides: all of the theories are correct. *Glycobiology* **3,** 97–130
7. Haltiwanger, R. S., and Lowe, J. B. (2004) Role of glycosylation in development. *Annu. Rev. Biochem.* **73,** 491–537
8. Guérardel, Y., Chang, L. Y., Maes, E., Huang, C. J., and Khoo, K. H. (2006) Glycomic survey mapping of zebrafish identifies unique sialylation pattern. *Glycobiology* **16,** 244–257
9. Ohtsubo, K., and Marth, J. D. (2006) Glycosylation in cellular mechanisms of health and disease. *Cell* **126,** 855–867
10. Solter, D., and Knowles, B. B. (1978) Monoclonal antibody defining a stage-specific mouse embryonic antigen (SSEA-1). *Proc. Natl. Acad. Sci. U.S.A.* **75,** 5565–5569
11. Kannagi, R., Cochran, N. A., Ishigami, F., Hakomori, S., Andrews, P. W., Knowles, B. B., and Solter, D. (1983) Stage-specific embryonic antigens (SSEA-3 and -4) are epitopes of a unique globo-series ganglioside isolated from human teratocarcinoma cells. *EMBO J.* **2,** 2355–2361
12. Lau, K. S., Partridge, E. A., Grigorian, A., Silvescu, C. I., Reinhold, V. N., Demetriou, M., and Dennis, J. W. (2007) Complex *N*-glycan number and degree of branching cooperate to regulate cell proliferation and differentiation. *Cell* **129,** 123–134
13. Lanctot, P. M., Gage, F. H., and Varki, A. P. (2007) The glycans of stem cells. *Curr. Opin. Chem. Biol.* **11,** 373–380
14. Surani, M. A. (1979) Glycoprotein synthesis and inhibition of glycosylation by tunicamycin in preimplantation mouse embryos: compaction and trophoblast adhesion. *Cell* **18,** 217–227
15. Akama, T. O., Nakagawa, H., Sugihara, K., Narisawa, S., Ohyama, C., Nishimura, S., O'Brien, D. A., Moremen, K. W., Millan, J. L., and Fukuda, M. N. (2002) Germ cell survival through carbohydrate-mediated interaction with Sertoli cells. *Science* **295,** 124–127
16. Shur, B. D., Rodeheffer, C., and Ensslin, M. A. (2004) Mammalian fertilization. *Curr. Biol.* **14,** R691–R692
17. Hato, M., Nakagawa, H., Kurogochi, M., Akama, T. O., Marth, J. D., Fukuda, M. N., and Nishimura, S. I. (2006) Unusual *N*-glycan structures in alpha-mannosidase II/IIx double null embryos identified by a systematic glycomics approach based on two-dimensional LC mapping and matrix-dependent selective fragmentation method in MALDI-TOF/TOF mass spectrometry. *Mol. Cell. Proteomics* **5,** 2146–2157
18. Eggens, I., Fenderson, B., Toyokuni, T., Dean, B., Stroud, M., and Hakomori, S. (1989) Specific interaction between Le^x and Le^x determinants. *J. Biol. Chem.* **264,** 9476–9484
19. Muramatsu, T., and Muramatsu, H. (2004) Carbohydrate antigens expressed on stem cells and early embryonic cells. *Glycoconj. J.* **21,** 41–45
20. Varki, A. (2007) Glycan-based interactions involving vertebrate sialic acid-

recognizing proteins. *Nature* **446,** 1023–1029
21. Martin, M. J., Muotri, A., Gage, F., and Varki, A. P. (2005) Human embryonic stem cells express an immunogenic nonhuman sialic acid. *Nat. Med.* **11,** 228–232
22. Takahashi, K., Tanabe, K., Ohnuki, M., Narita, M., Ichisaka, T., Tomoda, K., and Yamanaka, S. (2007) Induction of pluripotent stem cells from adult human fibroblasts by defined factors. *Cell* **131,** 861–872
23. Sakurada, K., McDonald, F. M., and Shimada, F. (2008) Regenerative medicine and stem cell based drug discovery. *Angew. Chem. Int. Ed. Engl.* **47,** 5718–5738
24. Pilobello, K. T., and Mahal, L. K. (2007) Deciphering the glycocode: the complexity and analytical challenge of glycomics. *Curr. Opin. Chem. Biol.* **11,** 300–305
25. Nishimura, S., Niikura, K., Kurogochi, M., Matsushita, T., Fumoto, M., Hinou, H., Kamitani, R., Nakagawa, H., Deguchi, K., Miura, N., Monde, K., and Kondo, H. (2004) High-throughput protein glycomics: combined use of chemoselective glycoblotting and MALDI-TOF/TOF mass spectrometry. *Angew. Chem. Int. Ed. Engl.* **44,** 91–96
26. Furukawa, J., Shinohara, Y., Kuramoto, H., Miura, Y., Shimaoka, H., Kurogochi, M., Nakano, M., and Nishimura, S. I. (2008) Comprehensive approach to structural and functional glycomics based on chemoselective glycoblotting and sequential tag conversion. *Anal. Chem.* **80,** 1094–1101
27. Edwards, M. K., Harris, J. F., and McBurney, M. W. (1983) Induced muscle differentiation in an embryonal carcinoma cell line. *Mol. Cell. Biol.* **3,** 2280–2286
28. Stanley, P. (2002) Biological consequences of overexpressing or eliminating *N*-acetylglucosaminyltransferase-TIII in mouse. *Biochim. Biophys. Acta* **1573,** 363–368
29. Gao, X., Bian, W., Yang, J., Tang, K., Kitani, H., Atsumi, T., and Jing, N. A. (2001) role of *N*-cadherin in neuronal differentiation of embryonic carcinoma P19 cells. *Biochem. Biophys. Res. Commun.* **284,** 1098–1103
30. Tang, K., Yang, J., Gao, X., Wang, C., Liu, L., Kitani, H., Atsumi, T., and Jing, N. (2002) Wnt-1 promotes neuronal differentiation and inhibits gliogenesis in P19 cells. *Biochem. Biophys. Res. Commun.* **293,** 167–173
31. Yagi, T., Tokunaga, T., Furuta, Y., Nada, S., Yoshida, M., Tsukada, T., Saga, Y., Takeda, N., Ikawa, Y., and Aizawa, S. (1993) A novel ES cell line, TT2, with high germ line-differentiating potency. *Anal. Biochem.* **214,** 70–76
32. Miura, Y., Hato, M., Shinohara, Y., Kuramoto, H., Furukawa, J., Kurogochi, M., Shimaoka, H., Tada, M., Nakanishi, K., Ozaki, M., Todo, S., and Nishimura, S. I. (2008) BlotGlycoABC™, an integrated glycoblotting technique for rapid and large scale clinical glycomics. *Mol. Cell. Proteomics* **7,** 370–377
33. McBurney, M. W., Jones-Villeneuve, E. M., Edwards, M. K., and Anderson, P. J. (1982) Control of muscle and neuronal differentiation in a cultured embryonal carcinoma cell line. *Nature* **299,** 165–167
34. Habara-Ohkubo, A. (1996) Differentiation of beating cardiac muscle cells from a derivative of P19 embryonal carcinoma cells. *Cell Struct. Funct.* **21,** 101–110
35. Inberg, A., Bogoch, Y., Bledi, Y., and Linial, M. (2007) Cellular processes underlying maturation of P19 neurons: changes in protein folding regimen and cytoskeleton organization. *Proteomics* **7,** 910–920
36. Baharvand, H., Piryaei, A., Rohani, R., Taei, A., Heidari, M. H., and Hosseini, A. (2006) Ultrastructural comparison of developing mouse embryonic stem cell- and *in vivo*-derived cardiomyocytes. *Cell Biol. Int.* **30,** 800–807
37. Wen, J., Xia, Q., Lu, C., Yin, L., Hu, J., Gong, Y., Yin, B., Monzen, K., Yuan, J., Qiang, B., Zhang, X., and Peng, X. (2007) Proteomic analysis of cardiomyocytes differentiation in mouse embryonic carcinoma P19CL6 cells. *J. Cell. Biochem.* **102,** 149–160
38. An, J., Yuan, Q., Wang, C., Liu, L., Tang, K., Tian, H. Y., Jing, N. H., and Zhao, F. K. (2005) Differential display of proteins involved in the neural differentiation of mouse embryonic carcinoma P19 cells by comparative proteomic analysis. *Proteomics* **5,** 1656–1668
39. Zamze, S., Harvey, D. J., Pesheva, P., Mattu, T. S., Schachner, M., Dwek, R. A., and Wing, D. R. (1999) Glycosylation of a CNS-specific extracellular matrix glycoprotein, tenascin-R, is dominated by O-linked sialylated glycans and "brain-type" neutral *N*-glycans. *Glycobiology* **9,** 823–831
40. Shimizu, H., Ochiai, K., Ikenaka, K., Mikoshiba, K., and Hase, S. (1993) Structures of *N*-linked sugar chains expressed mainly in mouse brain. *J. Biochem.* **114,** 334–338
41. Priatel, J. J., Sarkar, M., Schachter, H., and Marth, J. D. (1997) Isolation, characterization and inactivation of the mouse *Mgat3* gene: the bisecting *N*-acetylglucosamine in asparagines-linked oligosaccharides appears dispensable for viability and reproduction. *Glycobiology* **7,** 45–56

Osteoarthritis and Cartilage 18 (2010) 1133–1143

Osteoarthritis and Cartilage

OARSI OSTEOARTHRITIS RESEARCH SOCIETY INTERNATIONAL

Changes of human menisci in osteoarthritic knee joints

Y. Katsuragawa †‡, K. Saitoh †‡[a], N. Tanaka §, M. Wake §, Y. Ikeda §, H. Furukawa §, S. Tohma §, M. Sawabe ||, M. Ishiyama ¶, S. Yagishita ¶, R. Suzuki §, H. Mitomi #, N. Fukui §*

† *Department of Orthopaedic Surgery, National Center for Global Health and Medicine, Tokyo, Japan*
‡ *Department of Pathology, National Center for Global Health and Medicine, Tokyo, Japan*
§ *Clinical Research Center, National Hospital Organization, Sagamihara Hospital, Kanagawa, Japan*
|| *Department of Pathology, Tokyo Metropolitan Geriatric Hospital, Tokyo, Japan*
¶ *Department of Clinical Laboratory, Kanagawa Rehabilitation Hospital, Kanagawa, Japan*
# *Department of Pathology, Jyuntendo University School of Medicine, Tokyo, Japan*

ARTICLE INFO

Article history:
Received 16 November 2009
Accepted 29 May 2010

Keywords:
Osteoarthritis
Meniscus
IGF-1 (insulin-like growth factor-1)

SUMMARY

Objective: To investigate the changes of knee menisci in osteoarthritis (OA) in human.
Methods: OA and control menisci were obtained from 42 end-stage OA knees with medial involvement and 28 non-arthritic knees of age-matched donors, respectively. The change of menisci in OA was evaluated by histology, and gene expression of major matrix components and anabolic factors was analyzed in the anterior horn segments by quantitative PCR (qPCR). In those regions of menisci, the rate of collagen neo-synthesis was evaluated by [^{3}H]proline incorporation, and the change of matrix was investigated by ultrastructural observation and biomechanical measurement.
Results: In OA menisci, the change in histology was rather moderate in the anterior horn segments. However, despite the modest change in histology, the expression of type I, II, III procollagens was dramatically increased in those regions. The expression of insulin-like growth factor 1 (IGF-1) was markedly enhanced in OA menisci, which was considered to be responsible, at least partly, for the increase in procollagen gene expression. Interestingly, in spite of marked increase in procollagen gene expression, incorporation of [^{3}H]proline increased only modestly in OA menisci, and impaired collagen synthesis was suggested. This finding was consistent with the results of ultrastructural observation and biomechanical measurement, which indicated that the change of meniscal matrix was modest in the macroscopically preserved areas of OA menisci.
Conclusion: Although the expression of major matrix components was markedly enhanced, matrix synthesis was enhanced only modestly, and the changes of matrix in human OA menisci were rather modest in the non-degenerated areas.

Introduction

With the increasing human life expectancy, osteoarthritis (OA) has now become a leading cause of disability among older adults[1]. A knee joint is one of the most susceptible joints to OA, and OA of the knees accounts for a large part of the OA-related disability. In OA knees, almost all joint structures are affected by the disease. Knee menisci are also known to undergo an obvious change in OA[2].

Menisci are C-shaped fibrocartilaginous structures that are predominantly composed of type I, with small amounts of type II, type III collagens and proteoglycans[3–11]. Located between the femoral condyles and tibial plateau, menisci play important roles in load transmission, shock absorption, and maintenance of joint stability[12]. With the progression of OA, menisci undergo degenerative changes such as wearing and laceration[2]. Subluxation of menisci also occurs[13]. Reflecting their functional importance, the changes in menisci are closely associated with the initiation and progression of OA[14,15]. Although often studied in animal models, human OA menisci have seldom been the subject of investigation, and it is still not known well how menisci change in OA.

A meniscus is not a homogeneous tissue. Regional differences in tissue composition and cell metabolism have been observed between the inner and outer areas, and structural differences have been noticed between the surface and central regions[4,8–11,16–19]. Therefore, the evaluation of meniscus pathology would be more reasonably performed if such regional differences were considered.

* Address correspondence and reprint requests to: Naoshi Fukui, Clinical Research Center, National Hospital Organization, Sagamihara Hospital, Sakuradai 18-1, Sagamihara, Minami-ku, Kanagawa 252-0315, Japan. Tel/Fax: 81-42-742-8311.
E-mail address: n-fukui@sagamihara-hosp.gr.jp (N. Fukui).
[a] Deceased.

1063-4584/$ – see front matter
doi:10.1016/j.joca.2010.05.017

In this study, human menisci from OA and control knees were investigated by histological and molecular biological analyses, paying special attention to the regional differences within menisci. The rate of collagen neosynthesis was determined, and the change of meniscal matrix was evaluated by ultrastructural analysis and biomechanical measurement. The results of these analyses revealed the unique nature of the changes in human OA menisci, which are considerably different from those reported in animal studies.

Materials and methods

Material collection

This study was performed with the approval of the Human Ethics Review Committees of the participating institutions, and informed consent was obtained in writing from each subject or family of the donor before material collection. OA menisci were obtained in pairs of lateral and medial menisci from 42 OA knee joints of 40 patients within 4 h after a prosthetic surgery. The diagnosis of OA was based on the criteria of the American College of Rheumatology for OA[20], and all knee joints were medially involved in the disease. Control menisci were obtained from 28 non-arthritic knee joints of 22 donors (obtained bilaterally in six donors; ages 73–92 with a mean of 84) within 24 h after death. The donors were chosen from those who did not have a past record of treatment for joint disease or trauma, and the normality of the joint was confirmed macroscopically at the time of sample harvest. Prior to the analyses, all OA and control menisci were photographed and their macroscopic appearance was recorded. Control menisci were inspected closely, and were not used for the study if they showed overt signs of macroscopic degeneration. In this study, evaluations were performed on the anterior horn segments of menisci unless specified otherwise. This was because that those segments were well preserved in OA menisci, which made it possible to compare the changes in OA menisci directly in a site-to-site manner with those in the control menisci. Posterior horn segments of menisci were also often preserved in OA knees, but those segments were not used for the analyses. In this work, the OA and control menisci were randomly assigned to respective analyses. Some menisci were used for two or more evaluations.

Histological evaluation

Ten pairs of OA menisci and eight pairs of control menisci were used for this evaluation. The evaluation was performed primarily on the anterior horn segments of menisci, but for OA medial menisci, the body sections were also observed in order to know the changes in degenerated regions. Meniscus tissues were fixed in 4% paraformaldehyde, and 4-μm-thick sections were prepared in a plane perpendicular to the surface. The sections were stained with hematoxylin and eosin or Masson's trichrome stain, and observed under a light microscope. For the immunodetection of insulin-like growth factor (IGF)-1, the sections were pretreated with proteinase K (DakoCytomation, Carpinteria, California) and then incubated with a monoclonal antibody for human IGF-1 (Millipore, Billerica, Massachusetts). The primary antibody was reacted with the secondary antibody conjugated with streptavidine, which was visualized with 3,3′-diaminobenzidine (DAB), tetrahydrochloride using a commercially available kit (ChemMate EnVision Detection, DakoCytomation). The nuclei were stained with hematoxylin, and the localization of staining was observed under a light microscope.

Gene expression analysis

Twelve pairs of OA and control menisci were used for the evaluation. For the analysis, meniscus tissues were obtained from the anterior horn segments with a width of approximately 5 mm (Fig. 1). Immediately after harvest, the tissue was divided into four regions under a dissection microscope (Fig. 2). The divided tissues were each embedded in OCT compound (Sakura Finetechnical, Tokyo, Japan), snap frozen in liquid nitrogen, and stored at −80 °C until use. RNA was extracted from each of these regions by a previously described method[21]. cDNA was synthesized using the Sensiscript reverse transcriptase (Qiagen, Hilden, Germany) with a routine use of DNase I (Qiagen). Gene-specific primers and probes were prepared (Table I), and quantitative PCR (qPCR) was performed using either SYBR Premix Ex Taq or Premix Ex Taq (both from Takara Bio, Shiga, Japan) on a LightCycler (Roche Diagnostics, Basel, Switzerland). The expression levels were normalized by the expression of glyceraldehyde-3-phosphate dehydrogenase (*GAPDH*). For some samples, β-actin (*ACTB*) expression was also used for normalization.

Evaluation of collagen neosynthesis

The rate of collagen biosynthesis was determined by quantifying the amount of [^{3}H]proline incorporation into meniscus explants. Eight pairs of OA menisci and six pairs of control menisci were used for this analysis. The explants were prepared from the anterior horn segments of those menisci. In each of these menisci, the anterior horn segment was separated from the body segment, and the entire part of that segment was cut into 1–2 mm cubes, or explants. Four to six explants were placed in each of the 24-well tissue culture plates, which were maintained in Dulbecco's modified eagle medium (DMEM) containing 10% fetal bovine serum (FBS) and 25 μg/ml ascorbic acid. Forty-eight hours later, the media were then replaced by those containing 0.1% FBS, 25 μg/ml ascorbic acid and 10 μCi/ml [^{3}H]proline. After 8 h, the media were removed and the

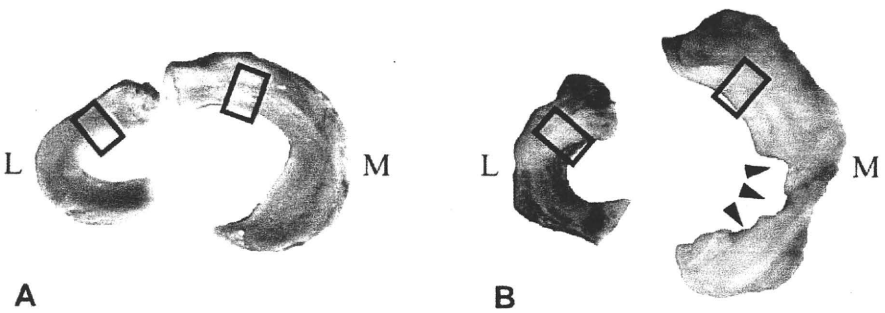

Fig. 1. Gross appearance of control and OA menisci. Representative photographs of control (A) and OA menisci (B) are shown. In each meniscus, a pair of parallel lines indicates the region in the anterior horn segment used for molecular biological analysis. In B, arrowheads indicate degenerated area in medial meniscus. M and L indicate medial and lateral menisci, respectively.